

# PUMP CAVITATION— VARIOUS NPSHR CRITERIA, NPSHA MARGINS, AND IMPELLER LIFE EXPECTANCY

by

**Bruno Schiavello**

Director Fluid Dynamics

Flowserve Pump Division

Applied Technology Department

Phillipsburg, New Jersey

and

**Frank C. Visser**

Principal Design & Fluid Dynamics Engineer

Flowserve Pump Division

Technical Services, Central Engineering

Etten-Leur, The Netherlands



*Bruno Schiavello has been Director for Fluid Dynamics at Flowserve Pump Division, Applied Technology Department, in Phillipsburg, New Jersey, since 2000, and previously served in the same position with Ingersoll Dresser Pump Company. He started in the R&D Department of Worthington Nord (Italy), joined Central R&D of Worthington, McGraw Edison Company, and then Dresser Pump Division.*

*Mr. Schiavello was co-winner of the H. Worthington European Technical Award in 1979. He has written several papers and lectured at seminars in the area of pump recirculation, cavitation, and two-phase flow. He is a member of ASME, has received the ASME 2006 Fluid Machinery Design Award, and has served on the International Pump Users Symposium Advisory Committee since 1983.*

*Mr. Schiavello received a B.S. degree (Mechanical Engineering, 1974) from the University of Rome, and an M.S. degree (Fluid Dynamics, 1975) from Von Karman Institute for Fluid Dynamics.*



*Frank C. Visser is Principal Design & Fluid Dynamics Engineer with Flowserve Pump Division, in Etten-Leur, The Netherlands. He joined Flowserve in 1995 (at that time, BW/IP International), where he was assigned to the company's Brite-Euram research project on advanced and preventive diagnosis of fluid-handling rotating machinery using artificial excitation and dynamic parameter identification*

*techniques (APHRODITE). Since then he has held several positions in research, development, and (product) engineering. His key expertise and interests relate to fluid mechanics and thermodynamics of (centrifugal) pumps and hydraulic turbines.*

*Dr. Visser obtained a B.S. degree (Mechanical Engineering, 1985) from Technical College Alkmaar, The Netherlands, and an M.S. degree (Mechanical Engineering, 1991) and Ph.D. degree (Technical Sciences, 1996) from the University of Twente, Enschede, The Netherlands. He is a member of the Royal Institution of Engineers in the Netherlands, and is the author of 20+ technical papers, published in journals and proceedings.*

## ABSTRACT

This tutorial deals with pump cavitation, discussing various net positive suction head required ( $NPSH_R$ ) criteria, net positive suction head available ( $NPSH_A$ ) margins and impeller life expectancy. It gives an introduction to the subject matter and provides insights on particulars like cavitation inception, 3 percent head drop, and 40,000 hours impeller life, as well as NPSH scaling laws. It further devotes attention to the effect of dissolved gases and thermal suppression (i.e., thermodynamic effect). With regard to numerical prediction capabilities the use of computational fluid dynamics (CFD) shall be discussed. Furthermore, guidance for cavitation damage diagnosis shall be given, including the peculiar aspects of various cavitation modes, the prediction of cavitation erosion rate, and assessment of impeller life expectancy. The tutorial will further address NPSHR criteria and NPSHA margin factors.

## INTRODUCTION

Cavitation is well recognized as a phenomenon that may cause serious pump malfunctioning due to improper pump inlet conditions. It is therefore important for the pump user to understand what cavitation is, what it potentially can cause, and how it can be controlled. This tutorial aims at providing such knowledge. It is oriented toward pump users and focuses primarily on cavitation in rotordynamic (centrifugal) pumps; though much of the discussion will hold in general.

The tutorial will start with an introductory overview, discussing in broad terms the physics of cavitation, and outlining the concept of net positive suction head (NPSH); in that some cavitation flow visualization footage will be used for additional clarification and illustration. The tutorial will further focus on (pump) cavitation related phenomena, such as performance deterioration, material damage from cavitation erosion, loss of priming, and vapor lock causing complete pump failure. As inherent phenomenon, suction recirculation onset will be addressed as well.

In connection to NPSH several other characteristic cavitation parameters often found in literature will also be discussed, including suction specific speed, the cavitation number, and the Thoma cavitation number. Typical critical values of these parameters, related to distinct phenomena and criteria, such as cavitation inception, percentage head loss, and 40,000 hour operation will be explained too.

In the context of cavitation predicting the tutorial will pay attention to scaling laws, impact of dissolved gases, thermodynamic effect caused by thermal suppression, and usage of computational fluid dynamics (CFD) to determine incipient cavitation, cavitation bubble length, and percentage head drop. Furthermore, guidance for cavitation damage diagnosis will be given, including the peculiar aspects of various cavitation modes, the prediction of cavitation erosion rate, and assessment of impeller life expectancy. Moreover modern tools available for impeller life enhancement will be highlighted, including the use of modern design impellers with special geometrical features, optimization with CFD, and in the case of upgraded material with high resistance to cavitation damage.

The tutorial will further address net positive suction head required (NPSHR) criteria and net positive suction head available (NPSHA) margin factors.

With the insights provided the pump user will have a better understanding of pump cavitation, and its potential for causing problems. The presented tools may assist the pump user in troubleshooting pump cavitation related phenomena. On the expert level the tools and insights can help to evaluate and enhance pump (impeller) designs, and make them less susceptible to cavitation.

## CAVITATION

Cavitation is defined as the process of formation and disappearance of the vapor phase of a liquid when it is subjected to reduced and subsequently increased pressures at constant ambient temperatures. The formation of cavities is a process analogous to boiling in a liquid, although it is the result of pressure reduction rather than heat addition. Nonetheless, the basic physical and thermodynamic processes are the same in both cases.

Clearly, from an engineering and design point of view there are two basic questions regarding cavitation. First, one has to answer the question whether cavitation will occur or not, and second, if cavitation is unavoidable, the question is whether a given design can still function properly. Economic or other operational considerations often necessitate operation with some cavitation, and under these circumstances it is particularly important to understand the (deleterious) effects of cavitation.

### Occurrence of Cavitation

A liquid is said to cavitate when:

- Vapor bubbles form and grow as a consequence of pressure reduction, and
- Vapor bubbles subsequently disappear or collapse due to a pressure increase.

Such bubble formation is nearly always accompanied by production of gases previously dissolved in the liquid. The phase transition resulting from the hydrodynamic pressure changes yields a two-phase flow composed of a liquid and its vapor phase, which is called a cavitating flow. Obviously, a cavitating flow can imply anything from the initial formation of bubbles to large-scale attached cavities (known as supercavitation). Such cavitating flows are rather common occurrences, since designers are pushing for higher speeds for given sizes in the development of pumps (thus creating lower pressure areas).

### Typical Cavitation Parameters

The potential for cavitation is typically evaluated in terms of cavitation parameters. Traditionally, the three most common cavitation parameters employed are:

- Cavitation number,  $\sigma$
- Net positive suction head, NPSH
- Thoma cavitation number,  $\sigma_{TH}$

*Cavitation number*—The cavitation number is defined as:

$$\sigma = \frac{p_1 - p_v}{\frac{1}{2} \rho U^2} \quad (1)$$

in which  $p_1$  is upstream static pressure,  $p_v$  is vapor pressure,  $\rho$  is fluid density, and  $U$  is a typical or reference velocity. For centrifugal pumps it is common to take the circumferential impeller eye velocity (i.e., inlet-vane tip speed) as reference velocity:  $U = U_e = \Omega R_{IT}$  with  $\Omega$  being the angular velocity and  $R_{IT}$  the inlet-vane tip radius.

*NPSH*—The NPSH is defined as the total head of the fluid—at the center line of the impeller—above the vapor pressure of the fluid, and can be regarded as a measure for the margin against vaporization of the fluid entering the pump. The formula to compute it reads:

$$NPSH = \frac{p_{01} - p_v}{\rho g} \quad (2)$$

in which  $p_{01}$  is upstream total pressure (i.e., including dynamic pressure), and  $g$  is acceleration due to gravity.

*Thoma number*—The Thoma cavitation number is defined as: in which  $H$  is total pump head.

$$\sigma_{TH} = \frac{NPSH}{H} \quad (3)$$

Although the cavitation number ( $\sigma$ ) can be regarded as the most fundamental cavitation parameter, one will find that in the context of pumps and (hydro) turbines, respectively, net positive suction head and net positive discharge head (NPDH) are typically used. The Thoma cavitation number is an archaic one, and is not particularly relevant to pump cavitation since this occurs at the inlet of a pump, which has little relation to the total head of a pump.

By using a parameter like the cavitation number, or the abstraction NPSH, one can define critical values at which certain cavitation phenomena occur. Typically, such phenomena are cavitation inception, percentage head drop, and performance breakdown.

### Cavitation Inception and Three-Percent Head Drop

The first appearance of cavitation is called cavitation inception. When the suction pressure—or available net positive suction head—is decreased from this inception level, the region of cavitation enlarges, eventually starting to cause noise, cavitation damage, performance change, head breakdown, loss of priming, and vapor lock.

By the time the inlet pressure is lowered enough to cause a certain percentage drop in pump head, cavitation is always fully established. Before reaching that stage there is already a significant amount of cavitation without the pump head being affected by it. Figure 1 illustrates the latter. It shows a leading edge sheet cavity, occurring well before any performance (i.e., pump head) deterioration takes place. This kind of situation is particularly inconvenient as it typically occurs near—or at—the point of maximum cavitation damage. This cavitation damage results from the fact that well beyond inception, the pressures associated with cavity collapse are high enough to cause failure of the impeller material. Near head breakdown the cavitation damage diminishes due to the cushioning effect of the surrounding bubbles of the fully developed cavitating flow. So, a point of maximum cavitation damage exists somewhere between inception and head breakdown.



Figure 1. Sheet Cavity on Centrifugal Pump Impeller Vane Leading Edge. (Courtesy of Visser, et al., 1998, Turbomachinery Laboratory)

Above-mentioned stages of cavitation are illustrated in Figure 2, in which the total pump head ( $H$ ) is plotted against the net positive suction head for constant volume flow rate ( $Q$ ) and constant speed ( $N$ ). From a set of test curves like Figure 2 it is possible to develop the NPSH required characteristic as a function of the through-flow. Such could be for instance the NPSH corresponding to three-percent head drop ( $NPSH_{3\%}$ , Figure 3). This is done by determining the cavitation point for 3 percent head drop at different ( $Q/N$ ) operating points, i.e., at different specific flow rates  $\Phi = Q/(\Omega R^3_{1T})$ . For multistage pumps this  $NPSH_{3\%}$  normally relates to the drop in head of the first stage.

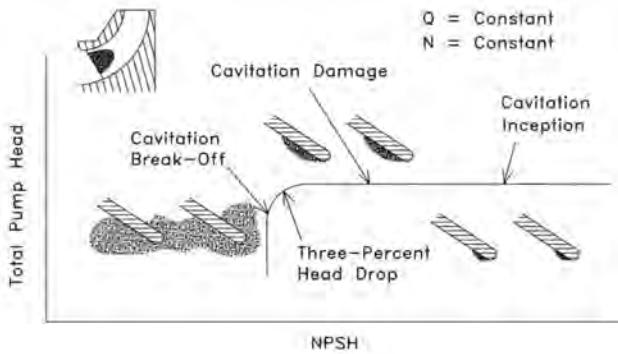


Figure 2. Cavitation Phenomena.

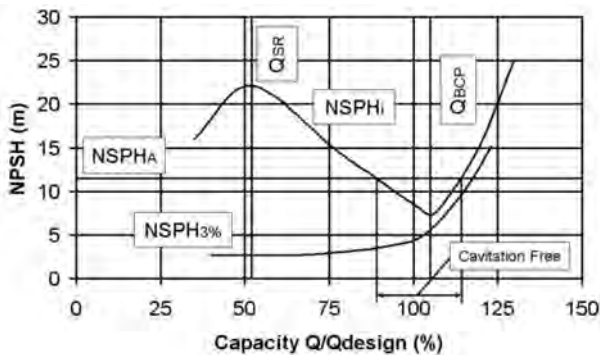


Figure 3. NPSH Characteristics.

Figure 3 shows typical NPSH characteristics that can be identified for centrifugal pumps. Beyond the so-called shockless-entry capacity—or best cavitation point (BCP)—the  $NPSH_{3\%}$  is seen to follow the steep rise of the inception curve ( $NPSH_i$ ). Below  $Q_{BCP}$  the inception curve rises until a local maximum is reached, which is associated with the onset of suction recirculation. It can further be seen that a cavitation free region of operation will exist for those capacities where  $NPSH_A > NPSH_i$ .

Besides incipient cavitation one may also encounter the term desinent cavitation, which relates to the situation at which cavitation disappears when the suction pressure of a cavitating flow is raised. Unless one has a hypothetical perfect fluid, desinent cavitation and incipient cavitation do not coincide, and any difference in associated cavitation numbers (or NPSH) is termed cavitation hysteresis (with  $\sigma_i < \sigma_d$ ).

Desinent cavitation tends to be more of an academic interest rather than being practical. Especially for (centrifugal) pumps, incipient cavitation has a much more relevant meaning since NPSH tests are done by gradually lowering pump suction pressure. So, inherently, incipient cavitation is the appropriate abstraction to be used for (centrifugal) pumps.

#### Cavitation Damage

Cavitation damage starts somewhere beyond inception and will disappear near head break-off, with maximum erosion rate occurring somewhere in between (refer to Figures 2 and 4). A more accurate description is difficult to give since many parameters influence bubble geometry and its potential for causing damage. For instance, impeller material, air content, NPSH available, vane geometry, inlet geometry, type of cavity, fluid density, and water temperature, to name a few, can be contributors or inhibitors of cavitation damage. The only certainty is that the absence of visible cavities means that cavitation damage will not be an issue. This fact is used in some conservative designs, such as liquid sodium pumps, and some water injection applications, where the NPSH available is high enough to suppress cavitation. In general, however, the designer pushes suction specific speeds (see below) to the point where suppression of (visible) cavitation is impossible and cavitation damage can be expected. Typical examples of cavitation damage on the vanes of a centrifugal pump impeller and a Francis type turbine runner are shown in Figures 5 and 6.

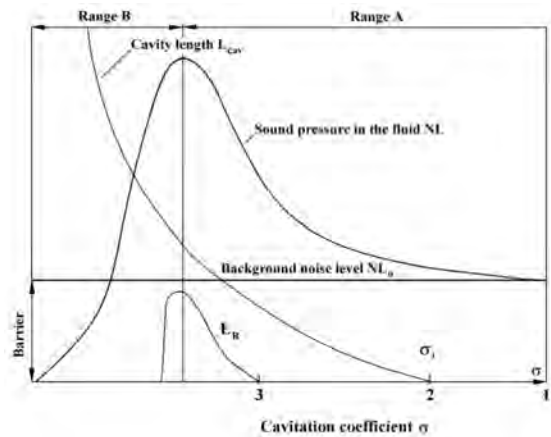


Figure 4. Acoustic Signal, Cavity Length, and Erosion Rate as Function of the Cavitation Coefficient; (1) Acoustic Inception, (2) Visual Inception, (3) Inception of Erosion. (Courtesy of Gülich, 1992)

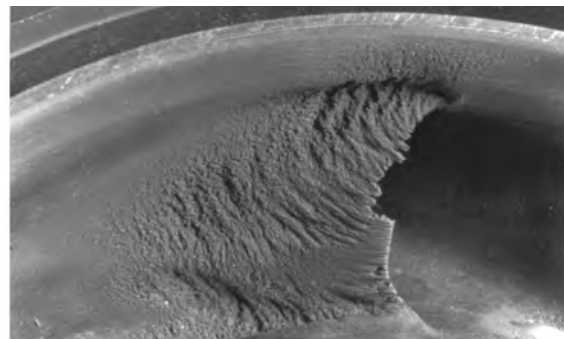


Figure 5. Typical Cavitation Damage: Centrifugal Pump Impeller with Cavitation Erosion at Vane Inlet. (Courtesy of Gülich and Rösch, 1988)

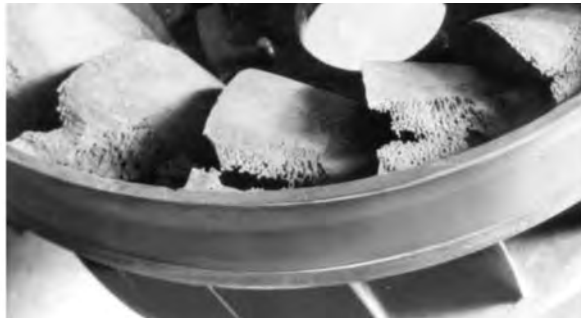


Figure 6. Typical Cavitation Damage: Francis Turbine Runner with Serious Cavitation Damage at Runner Discharge. (Courtesy of Brennen, 1994)

Suction Specific Speed

The suction specific speed (S) determines the susceptibility to cavitation, and is defined (see for instance Brennen, 1994) as:

$$S = \Omega Q^{1/2} / (NPSE)^{3/4} \tag{4}$$

in which NPSE is the net positive suction energy (gNPSH).

Like the common specific speed,  $\Omega_s = \Omega Q^{1/2} / (g H)^{3/4}$ , the suction specific speed is a dimensionless number, and should (preferably) be computed using a consistent set of units. A typical (i.e., critical) value for the suction specific speed, using consistent units, is  $S_c = 3.0$  (Dixon, 1978) (Table 1). In traditional US evaluation this critical value ( $S_c$ ) equals about 8200. It should be recognized that this critical suction specific speed of 3.0 (8200 US) is often erroneously seen as the value at inception ( $S_i$ ). As a matter of fact, operation below the critical value ( $S_A < S_c$ ) will imply the absence of cavitation or cavitation damage only if  $S_c = S_i$ .

Table 1. Comparison of Inception ( $S_i$ ) and Breakdown ( $S_b$ ) Suction Specific Speed for Some Typical Pumps (Adapted from Brennen, 1994, after McNulty and Pearsall, 1979); the Numbers Between Parentheses Denote US Customary Values.

Pump Type	$\Omega_s$	Flow $Q/Q_B$	$S_i$	$S_b$	$S_b/S_i$	$\frac{NPSH_i}{NPSH_b}$
Process pump with volute and diffuser	0.31	0.24	0.25 (684)	2.0 (5469)	8.0	16
	(848)	1.20	0.8 (2188)	2.5 (6837)	3.1	4.5
Double entry pump with volute	0.96	1.00	0.6 (1641)	2.1 (5743)	3.5	5.3
	(2625)	1.20	0.8 (2188)	2.1 (5743)	2.6	3.6
Centrifugal pump with diffuser and volute	0.55	0.75	0.6 (1641)	2.41 (6590)	4.0	6.3
	(1504)	1.00	0.8 (2188)	2.67 (7301)	3.3	4.9
Cooling water pump	1.35	0.50	0.65 (1777)	3.4 (9298)	5.2	9.0
		0.75	0.6 (1641)	3.69 (10091)	6.2	11.4
		1.00	0.83 (2270)	3.38 (9243)	4.1	6.6
Volute pump	1.00	0.60	0.76 (1996)	1.74 (4758)	2.3	3.0
		1.00	0.83 (2270)	2.48 (6782)	3.0	4.3
		1.20	1.21 (3309)	2.47 (6754)	2.0	2.5

The last column of Table 1 shows the  $NPSH_i/NPSH_b$  ratio as derived from  $S_b/S_i$ , using Equation (4). It clearly shows that inception occurs well before the pump head breaks down; that is, at suction pressures several times the value associated with head breakdown.

Caution: Suction specific speed is a relative index number that should be used and judged with extreme caution. In order to have some consistency the widespread rule is that it should be evaluated at the pump's peak efficiency capacity, with maximum diameter impeller fitted in the pump. Although this leads to a workable definition in practice, it has some serious drawbacks:

- The volute or diffuser characteristic will greatly determine the peak efficiency capacity of a centrifugal pump (for instance, Worster, 1963).
- For multistage pumps the series stages may have a peak efficiency capacity quite different from the first stage.

This makes S (very) sensitive to the construction of the entire pump, whereas it should only reflect the suction capabilities. A way to overcome this objection is to evaluate S at the so-called shockless entry capacity of the suction impeller.

Cavitation Erosion and  $NPSH_{40,000}$

In order to have cavitation erosion, three conditions must exist:

- Cavitation bubbles must form in the fluid ( $S_A > S_c$ ),
- Cavitation bubbles must implode on or very near the vane surface, and
- Cavitation intensity must exceed the cavitation resistance of the surface material.

While the first two points above are relatively easy to ascertain visually, the third point is rather hard to quantify. Therefore, many experimental and semi-empirical studies have attempted to correlate between cavity shape and damage potential (e.g., Gülich and Pace, 1986; Gülich and Rösch, 1988; Gülich, 1989a, 1989b). Additionally, several others have applied a somewhat informed approach to predict NPSH requirements. For instance, a time-honored method is the one proposed by Vlaming (1981, 1989). His NPSH required for 40,000 hour impeller life at the shockless entry point is given as:

$$NPSH_{SE,40} = (k_1 C_{m1}^2 + k_2 W_1^2) / 2g \tag{5}$$

where  $k_1$  has constant value of 1.2,  $C_{m1}$  is upstream meridional velocity,  $W_1$  is upstream relative velocity, and  $k_2 = 0.28 + (U_c [ft/s]/400)^4$ . This relation reflects a fundamental correlation, with coefficients  $k_1$  and  $k_2$  based on empirical data.

Since Equation (5) gives  $NPSH_R$  for 40,000 hours of impeller life at shockless capacity, one will need to take the effect of incidence into account for other capacities. This can be expressed as:

$$NPSH_{40} = NPSH_{SE,40} + \Delta NPSH_{40} \tag{6}$$

Following the empirical model of Vlaming (1981, 1989), the incidence effect is (refer also to Cooper, et al., 1991):

$$\Delta NPSH_{40} = f NPSH_{SE,40} \{ (NPSH_{SE,40} [ft])^{0.105} - 1 \} \tag{7}$$

where:

$$f = \begin{cases} 0.887q + 0.893q^2 & \text{for } Q < Q_{SE} \\ -2.82q + 6.61q^2 & \text{for } Q > Q_{SE} \end{cases} \tag{8}$$

with  $q = (Q_{SE} - Q)/Q_{BEP}$  and the subscript  $BEP$  denoting best efficiency point.

It is believed that for reasonably good designs, adherence to NPSH values as calculated above would ensure an impeller life of 40,000 hours against cavitation damage. Figure 7 shows a typical example of  $NPSH_R$  calculated for 40,000 hours impeller life.

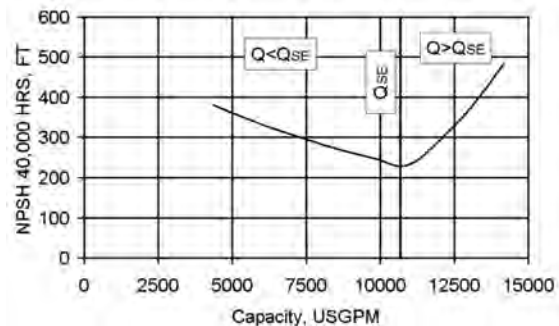


Figure 7. Example  $NPSH_R$  for 40,000 Hours Impeller Life;  $N = 3600$  RPM;  $D_{eye} = 11\frac{3}{4}$  in,  $d_{hub} = 7\frac{1}{2}$  in,  $b_{eye} = 18$  Degrees,  $c_{1u}/u_{eye} = 0.1$  (10 Percent Rerotation).

Remark: on a personal (critical) note the coauthor questions the appropriateness of using  $q = (Q_{SE} - Q)/Q_{BEP}$  in Equation (8), since a pump's BEP has little to do with suction performance. The BEP of a pump is primarily determined by the combination of its volute or diffuser characteristic and the impeller discharge characteristic (Worster, 1963); it holds little relation with suction performance. As such, the coauthor tends to use  $q = 1 - Q/Q_{SE}$ .

#### Cavity Length Damage Correlation

Although the concept of  $NPSH_{40,000}$  is easy to use it is more appropriate from a physical standpoint to focus on (predicting) the erosion rate in relation to the amount of developed cavitation. A method that does the latter, receiving wide attention over the last two decades, is the one developed by Gülich (Gülich and Pace, 1986; Gülich and Rösch, 1988; Gülich, 1989a, 1989b). His correlation is based on the bubble or cavity length  $L_{cav}$  and can be stated as (Cooper, et al., 1991):

$$E = C \left( \frac{L_{cav}}{L_{cav,10}} \right)^n \left( \tau_A - \phi^2 \right)^3 U_e^6 \rho^3 A (8T_S^2)^{-1} \quad (9)$$

with:

$$\tau_A = 2g NPSH_A / U_e^2 \quad (10)$$

where E is erosion rate in (mm/h),  $L_{cav,10}$  is reference bubble length of 10 mm (0.3937 in), n is 2.83 for blade suction side and 2.6 for blade pressure side,  $\phi$  is inlet flow coefficient ( $C_{m1}/U_e$ ),  $U_e$  is eye velocity in (m/s),  $\rho$  is fluid density in (kg/m<sup>3</sup>),  $T_S$  is tensile strength of impeller material in (Pa), and:

$$A = \begin{cases} 1 & \text{for cold water} \\ 0.705 & \text{for } 175^\circ\text{C}/347^\circ\text{F boiler feed water} \end{cases}$$

and:

$$C = \begin{cases} 7.92 \cdot 10^{-6} \text{ mm h}^{-1} \text{ Pa}^{-1} & \text{for blade suction side } (C_{SS}) \\ 3.96 \cdot 10^{-4} \text{ mm h}^{-1} \text{ Pa}^{-1} & \text{for blade pressure side } (C_{PS}) \end{cases}$$

Empirical correlation (9) enables assessment of cavitation erosion impact and lifetime expectancy if the size of the cavity is known. Typically, the correlation derived by Gülich (9) is used to state that a depth penetration of 75 percent of the blade thickness, t, constitutes the end of useful life of the impeller in question; that is, after 0.75 t/E hours. The correlation further reveals that occurrence of cavitation is most severe (in terms of damage potential) on the blade pressure side ( $C_{PS} = 50 C_{SS}$ ).

Although the damage rate (E), as indicated above, is affected by a number of factors, it can be argued that a usable correlation can be deducted with cavity length as the primary independent variable; i.e.:

$$E \propto L_{cav}^n \quad (11)$$

This particular relation provides a very reasonable basis to project a change in impeller life when the impeller (vane) geometry is modified, while all other factors remain (practically) unchanged (Ferman, et al., 1997; Visser, et al., 1998).

#### CAVITATION PREDICTION

Cavitation is a key design consideration for centrifugal pumps and their application. Hence, it is important to be able to predict if—and how much—cavitation can be expected, and evaluate whether this might cause operational problems for a particular application. To that end, means and insights will be presented here, which may assist both the pump designer and the application engineer or pump user in handling cavitation related issues. Particulars that will be discussed include:

- Scaling laws.
- Thermodynamic effect (from thermal depression).
- Effect of dissolved gases.
- Calculation of incipient cavitation ( $NPSH_i$ ) from CFD.
- Cavity length prediction using CFD.

#### Scaling Laws

A time-honored means to scale NPSH follows from combining Equations (1) and (2), which yields:

$$\frac{g NPSH}{\frac{1}{2} U^2} = \sigma + \phi^2 \quad (12)$$

For centrifugal pumps this relation has been translated to the affinity law:

$$\frac{NPSH}{N^2} = \text{constant} \quad (13)$$

which implies/assumes that  $\sigma$  and  $\phi$  are constant for a given flow situation and fixed fluid properties; that is,  $\sigma = \sigma(\phi) = \text{constant}$ .

Traditionally, Equation (13) forms the basis for predicting centrifugal pump NPSH requirements at a certain pump speed, using data at another (baseline) speed or model test speed. Unfortunately, however, there are many complex factors influencing inception and development of cavitation (refer, for instance, to Brennen, 1994, 1995), which may result in a significant departure from the affinity law (13). As such, one should be cautious when using Equation (13) to scale NPSH.

One important factor to consider when scaling NPSH with pump speed is the residence time, or mechanical time (say,  $t_m$ ) available for cavitation development (i.e., cavity/bubble growth). If the cavity growth is dominated by the mechanical time,  $t_m$ , and not by thermodynamic effects (see below), one will likely experience that  $NPSH_R$  at high speed is less than predicted per Equation (13)—and, vice versa, more for low speed. This holds the risk that  $NPSH_R$  at low speed may turn out to be (much) higher than anticipated per equation (13), which may cause a centrifugal pump to fail to operate (properly) at low speed if  $NPSH_A$  is insufficient because a lower  $NPSH_R$  was anticipated.

A typical approach to account for residence time effect when scaling NPSH with speed is for instance to use a modified version of Equation (13), yielding:

$$\frac{NPSH}{N^\alpha} = \text{constant} \quad (14)$$

with  $1 \leq \alpha \leq 2$ . The choice of  $\alpha$  is rather arbitrary and relies heavily on empiricism (and the experience of the pump designer and pump user). Equation (14) will yield conservative estimates (application-wise) when using  $\alpha = 1$  when going down in speed and  $\alpha = 2$  when going up in speed. The latter has the drawback that a high speed pump may be oversized for meeting the projected  $NPSH_R$ .

Another way of scaling NPSH is given by Tenot's equation. This correlation reads (see for instance Stepanoff, 1965):

$$\frac{\sigma_{TH,1} - \sigma_{TH}^*}{\sigma_{TH,2} - \sigma_{TH}^*} = \frac{H_2}{H_1} \quad (15)$$

in which  $\sigma_{TH}^*$  is called critical sigma. To employ Equation (15) one needs to know  $\sigma_{TH}^*$ , which can be determined from two (baseline) tests at significantly different speeds. To that end Equation (15) can be rephrased as:

$$\sigma_{TH}^* = \frac{NPSH_1 - NPSH_2}{H_1 \left\{ 1 - \left( \frac{N_2}{N_1} \right)^2 \right\}} \quad (16)$$

where NPSH is, for instance, the value corresponding to 3 percent head drop.

After establishing  $\sigma_{TH}^*$  one can compute NPSH at other speeds using Equation (15), which is thereto transformed to:

$$NPSH(N) = NPSH_{REF} - \sigma_{TH}^* H_{REF} \left\{ 1 - \left( \frac{N}{N_{REF}} \right)^2 \right\} \quad (17)$$

in which the subscript REF denotes the reference or baseline value.

*Example*—A pump is tested at 1500 rpm and 3000 rpm. At 1500 rpm the head is 25 m (82 ft) and the NPSH<sub>R</sub> is 4 m (13.1 ft). At 3000 rpm the head is 100 m (328 ft) and the NPSH<sub>R</sub> is 10 m (32.8 ft). This yields per Equation (16) that  $\sigma_{TH}^*$ . Then, for instance, at 2200 rpm this gives NPSH<sub>R</sub> = 6.3 m (20.7 ft). Scaling up quadratically from 1500 rpm would give NPSH<sub>R</sub> = 8.6 m (28.2 ft) at 2200 rpm, which overpredicts NPSH<sub>R</sub> by 36.5 percent. Scaling quadratically down from 3000 rpm would give NPSH<sub>R</sub> = 5.4 m (17.7 ft) at 2200 rpm, which underpredicts NPSH<sub>R</sub> by 14.3 percent. The latter holds the risk of serious cavitation, and even performance failure (i.e., when 5.4 m < NPSH<sub>A</sub> < 6.3 m).

*Thermodynamic Effect (Thermal Depression)*

Apart from residence or mechanical time,  $t_m$ —as discussed in the previous section—the development of cavitation may also be affected by thermodynamic effects, coming from thermal depression.

It will be evident that a change in temperature of the pumped liquid will affect the vapor pressure and therefore the NPSH or cavitation number. There is, however, another—more important—effect that relates to the underlying mechanism of heat and interface mass transfer associated with cavitation. Figures 8, 9, and 10 illustrate this effect for water pumped at different temperatures.

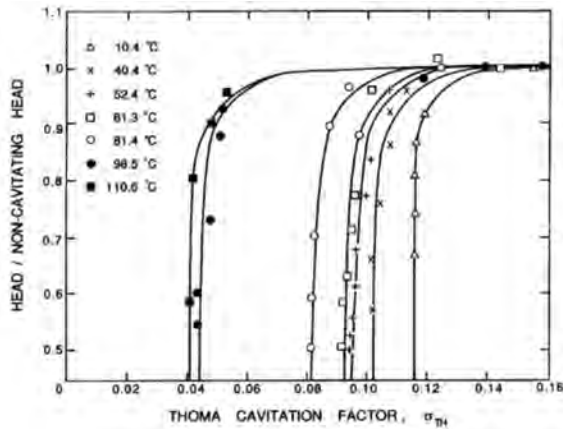


Figure 8. Thermodynamic Effect on Cavitation. (Head Drop Curves from Chivers, 1967, 1969, Test Series 1 adapted from Brennen, 1994, respectively, Arndt, 1981, with Correction per Original Graph of Chivers, 1967)

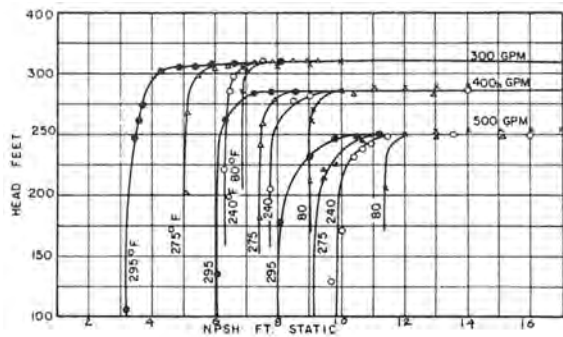


Figure 9. Thermodynamic Effect on Cavitation; Head Drop Curves. (Courtesy of Stepanoff, 1965)

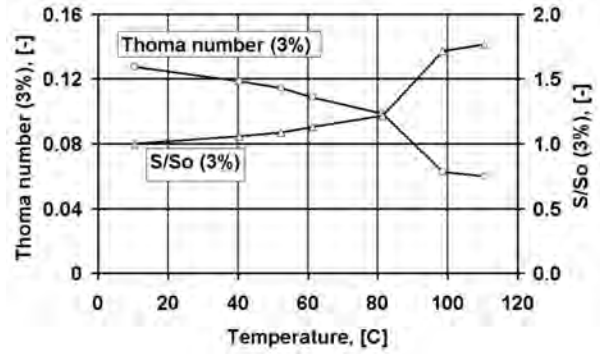


Figure 10. Thermodynamic Effect on Cavitation; Effect of Temperature on  $\sigma_{TH,3\%}$  and Suction Specific Speed ( $S/S_0$ ) as Derived from Figure 6.

Figures 8 and 9 present head drop curves for water pumped at elevated temperatures. The graphs show that pumping high temperature water requires less NPSH. Figure 8 displays  $\sigma_{TH,3\%}$  and  $S/S_0$  as function of temperature, as derived from Figure 8 using the proportionality relation  $S \propto \sigma_{TH}^{-3/4}$ . The graph demonstrates that suction specific speed,  $S$ , increases with temperature. First there is a region of gradual increase, followed by a more steep rise and then again a gradual increase. Now looking, for instance, at water of 230°F (110°C), one sees that suction specific speed at that particular temperature is 175 percent of the cold water value ( $S_0$  at 50°F, 10°C). This is an important observation because many pump users place a maximum limit on the suction specific speed that a pump may have. Such limit, however, can be totally inappropriate for hot applications, as well as for applications pumping liquids other than water. The thermodynamic effect lowers the NPSH<sub>R</sub>, and increases the suction specific speed (significantly).

When pumping hot water or liquids other than water (e.g., hydrocarbons), the thermodynamic effect yields:

$$NPSH_R^{(2)} = NPSH_R^{(1)} - \Delta NPSH \quad (18)$$

with  $\Delta NPSH \geq 0$ . In Equation (18) NPSH<sub>R</sub> relates to a certain amount of performance breakdown (e.g., 3 percent head drop), and the subscripts (1) and (2) denote reference or test value, and corrected or depressed value, respectively.

Based on equilibrium theory (see for instance Stepanoff, 1965) it is found that the reduction in NPSH equals:

$$\Delta NPSH = B \frac{\rho_L v_{fg}^2}{\rho_V^2 v_{fg}^2 g C_p T} \quad (19)$$

in which B is vapor-to-liquid ratio in the impeller eye associated with a certain performance breakdown,  $\rho_L$  is liquid density,  $\rho_V$  is vapor density,  $h_{fg}$  is latent heat of evaporation ( $h_V - h_L$ ),  $v_{fg}$  is the difference in specific volume between vapor and liquid phase ( $v_V - v_L$ ),  $C_p$  is (fluid) specific heat, and T is bulk temperature of the fluid. The essence of the theory leading to Equation (19) is that there is a necessary temperature depression in the liquid to produce the vapor. Equation (19) establishes a basis to predict the change in NPSH<sub>R</sub> due to thermodynamic effect.

Following Stepanoff (1965), Equation (18) becomes by asymptotic approximation:

$$\Delta NPSH \sim B/B_1 \quad (20)$$

as  $\rho_V / \rho_L \rightarrow 0$ , where:

$$B_1 = \left( \frac{\rho_L}{\rho_V} \right)^2 \frac{g C_p T}{h_{fg}^2} \quad (21)$$

The group denoted by  $B_1$  captures the relevant thermophysical properties of the fluid and the influence of temperature. It is a

parameter that plays a key role in nearly all analyses of thermodynamic effects on cavitation. The parameter  $B_1$  is not dimensionless, but has the dimension of a reciprocal length scale, e.g.,  $(\text{m}^{-1})$  or  $(\text{ft}^{-1})$ .

On the basis of Equation (20) Stepanoff (1965) investigated the NPSH behavior of various liquids and hot water leading to his empirical correlation:

$$\Delta NPSH = \begin{cases} \frac{29}{H_V} (B_1 [\text{m}^{-1}])^{-3/4} \\ \frac{64}{H_V} (B_1 [\text{ft}^{-1}])^{-3/4} \end{cases} \quad (22)$$

with  $H_V$  being the vapor pressure expressed in height of liquid column  $([\text{m}^{-1}]$  or  $[\text{ft}^{-1}]$ ). Equation (22) provides a means to obtain the cavitation performance under a given condition by applying the shift expressed by Equation (18).

*Example*—A pump that has been selected to pump boiler feedwater of 174°C (345°F) has an  $NPSH_R$  of 10 m (32.8 ft) at duty capacity when pumping cold water. The thermophysical properties of water at 345.2°F (174°C) are:  $\rho_L = 893.3 \text{ kg/m}^3$ ,  $r_V = 4.51 \text{ kg/m}^3$ ,  $C_p = 4.383 \text{ kJ/kg K}$ ,  $h_{fg} = 2035 \text{ kJ/kg}$ , and  $p_v = 871.6 \text{ kPa}$ . This gives per Equation (21) that  $B_1 = 0.182 \text{ (m}^{-1})$  ( $0.055 \text{ [ft}^{-1}]$ ), which yields per correlation (21) that one may expect an  $NPSH_R$  reduction of  $\Delta NPSH = 2.8 \text{ m}$  (9.3 ft). Hence, the  $NPSH_A$  can be significantly less than anticipated per cold water value.

Following the graphical method of the Hydraulic Institute (ANSI/HI 1.3, 2000), one would find for this particular example an NPSH reduction of about 2.1 m (6.9 ft). This is in line with the one calculated in the example. The graphical method of the Hydraulic Institute is easier to use, but the author's recommendation is to use it solely in order to obtain an approximate guess of the NPSH reduction, because it is less accurate than the method outlined above.

#### Dissolved Gases

Dissolved gases can have a major (detrimental) affect on the cavitation performance of centrifugal pumps. The release and expansion of dissolved gases can cause performance breakdown at suction pressures well above the ones corresponding to the established liquid  $NPSH_R$  (i.e., from the vendor's pump test). Hence, the pure liquid vapor pressure is unsuited to evaluate NPSH. Instead, an effective or artificial vapor pressure,  $p_E$ , should be used (Tsai, 1982):

$$p_E = p_V + \Delta \quad (23)$$

with  $\Delta > 0$ . Following Chen (1982) the effective vapor pressure is calculated as a fraction,  $y$ , of the upstream pressure,  $p_1$ :

$$p_E = yp_1 \quad (24)$$

with:

$$y = \frac{b + \sqrt{b^2 - 4ac}}{2a} \quad (25)$$

and:

$$a = \mu(1 - R) + 1 \quad (26)$$

$$b = 2\mu R(1 - R) + 1 \quad (27)$$

$$c = \mu R^2(1 - R) \quad (28)$$

with:

$$\mu = [\xi(1 - \xi)]/s \quad (29)$$

and:

$$R = p_V / p_1 \quad (30)$$

where  $\xi$  is (allowable) volume fraction of vapor at the impeller eye (typically 2 to 3 percent), and  $s$  is solubility factor:

$$s = x_G \rho_L / \rho_{G0} \quad (31)$$

in which  $x_G$  is mass fraction of dissolved gas upstream of the pump at pressure  $p_1$ , and  $\rho_{G0}$  is density of the gas at upstream pressure ( $p_1$ ) and temperature ( $T_1$ ).

Equation (27) holds for conservative calculations, in which the liquid is normally assumed to be saturated with dissolved gas. If so desired—and when appropriate—the calculation can be further refined by including the saturation factor (refer to Chen, 1982; or Wood, et al., 1998).

In summary, the procedure to evaluate the influence of dissolved gas is to calculate in consecutive order:  $s$ ,  $R$ ,  $\mu$ ,  $y$ , and  $p_E$ , and then determine  $NPSH_A$  from:

$$NPSH_A = \frac{p_{01} - p_E}{\rho g} \quad (32)$$

For proper operation this  $NPSH_A$  should exceed the  $NPSH_R$  of the pump. Wood, et al. (1998), further recommend a minimum margin ( $NPSH_A - NPSH_R$ ) of 5 ft, or 1.35 times the  $NPSH_R$ , whichever is greater.

*Example*—A centrifugal pump has to pump a hydrocarbon mixture with 0.1 mass% dissolved carbon dioxide ( $\text{CO}_2$ ). The hydrocarbon has a specific gravity (SG) of 0.900 and the  $\text{CO}_2$  SG at pump suction pressure and temperature is 0.00104. The suction pressure is 6 bar(abs) (87 psia) and the vapor pressure is 1 bar(abs) (14.5 psia). Following the method of Chen (1982) described here above the effective vapor pressure,  $p_E$ , is found to be 5.2 bar(abs) (75.4 psia), i.e.,  $y = 0.867$ . This results in an  $NPSH_A$  of 9.0 m (29.5 ft), which is almost 85 percent less than the value based on the hydrocarbon vapor pressure (yielding 56.6 m [186 ft]!).

#### Cavitation and Computational Fluid Dynamics

*Incipient cavitation ( $NPSH_i$ )*—The incipient cavitation characteristic plays a key role when designing and evaluating centrifugal impellers with regard to suction performance. As discussed earlier (refer to Figure 2) pumps can—and will—operate satisfactorily for a certain period of time when  $NPSH_R < NPSH_A < NPSH_i$ . However, there may be applications where it is desired to have  $NPSH_i < NPSH_A$  over a particular flow range (refer to Figure 3) and thus ensure a cavitation free region of operation. The objective of the pump designer will then be to establish a design with its best cavitation point somewhat beyond the design operating capacity,  $Q_{\text{design}}$ , and have  $NPSH_i < NPSH_A$ . Depending on the desired run-out capacity and the volumetric efficiency of the pump/impeller combination the ratio  $Q_{\text{BCP}}/Q_{\text{design}}$  can be up to 120 to 125 percent, or even further. A high  $Q_{\text{BCP}}/Q_{\text{design}}$  ratio, however, places a serious constraint on the  $NPSH_i$  that can be met at design capacity, and may even make it impossible to achieve  $NPSH_i < NPSH_A$  at  $Q_{\text{design}}$ .

To determine the incipient cavitation characteristic there are several options, including:

- Flow visualization.
- Hydro-acoustic noise measurement.
- Numerical flow simulations.

Flow visualization requires dedicated test setups to be built, which tend to be time consuming and costly. Hydro-acoustic noise measurement is easier to conduct (and to some extent less costly) than flow visualization, but accuracy and reliability are less. Numerical flow simulation is the most economical way, but produced results should be considered with appropriate care as there can be many sources of error (e.g., modeling compromises, grid influences, and numerical error, to name a few). Nonetheless, numerical flow simulation, or computational fluid dynamics is becoming more and more important and practical.

When employing CFD to simulate the flow through a centrifugal pump/impeller it is a matter of running a simple post-processing step to obtain the  $NPSH_i$  associated with the capacity for which the CFD was run. By definition one has:

$$NPSH_i = \frac{p_{01,i} - p_v}{\rho g} \quad (33)$$

where  $p_{01,i}$  is the total upstream (suction) pressure, associated with the situation that cavitation starts somewhere downstream. This total pressure equals:

$$p_{01,i} = p_{1,i} + \frac{1}{2} \rho C_1^2 \quad (34)$$

in which  $p_{1,i}$  is upstream static (suction) pressure corresponding to the situation that cavitation starts somewhere downstream, and  $C_1$  is inlet velocity (refer also to Figure 11).

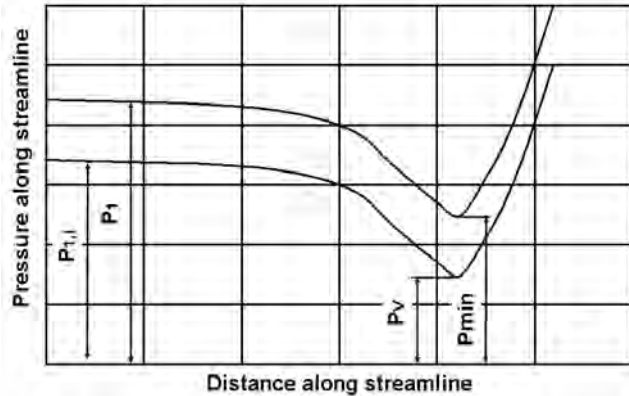


Figure 11. Streamline Through Point of Minimum Pressure at the Entrance of an Impeller.

With reference to Figure 11 it further follows from the principle of superposition that:

$$p_1 - p_{1,i} = p_{min} + p_v \quad (35)$$

or:

$$p_{1,i} = p_1 - (p_{min} + p_v) \quad (36)$$

in which  $p_{min}$  is minimum pressure at a particular location downstream. The principle of superposition, as used above, is inherently connected to the governing (Navier-Stokes) equations since these contain the pressure gradient only; so any constant pressure offset will not alter the (single phase) CFD computed (velocity) flow field.

Next substituting Equation (36) in Equation (34) one gets:

$$p_{01,i} = p_{01} - (p_{min} - p_v) \quad (37)$$

where  $p_{01} = p_1 + \frac{1}{2} \rho C_1^2$ . Substituting Equation (37) in Equation (33) then gives:

$$NPSH_i = \frac{p_{01} - p_{min}}{\rho g} \quad (38)$$

Equation (38) states that incipient NPSH can be readily calculated if one knows the total upstream (suction) pressure,  $p_{01}$ , and the minimum pressure,  $p_{min}$ , at a particular location downstream. Equation (38) further indicates that one does not need to know the vapor pressure to determine the incipient NPSH. This is a logical consequence of the definition of NPSH, which represents the net margin between (total) suction pressure and vapor pressure.

Figure 12 shows an exemplary result of  $NPSH_i$  calculated from CFD per Equation (38) and the  $NPSH_i$  determined experimentally (from model test flow visualization).

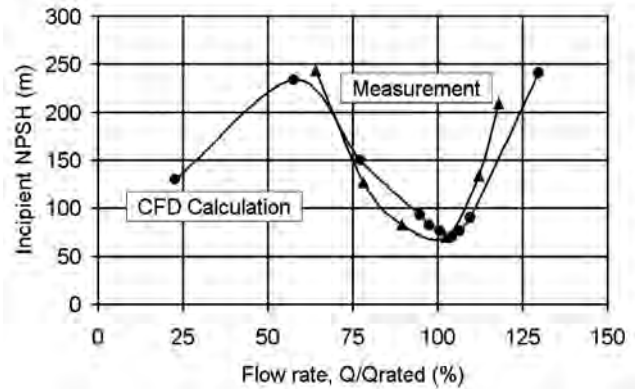


Figure 12. Example of CFD Calculated  $NPSH_i$  (●), Compared to Measurements (▲). (Courtesy of Visser, 2001)

The formulation given above, i.e., Equation (38), will hold for a hypothetical flow of liquid that cannot withstand any tension, and in which cavitation bubbles appear instantaneously when local static pressure ( $p$ ) reaches the vapor pressure ( $p_v$ ). Real fluids may deviate considerably from this behavior, and actual inception for real fluids may be significantly different from the value determined per Equation (38). Reasons for inception taking place below or above the  $NPSH_i$  given by Equation (38) include:

- Existence of tensile strength, causing a reduction in inception level.
- Residence time effects, causing a reduction in inception level.
- Dissolved gases, causing an increase in inception level.
- Turbulence effects, causing an increase in inception level.

Without these effects the prediction of inception level would be a straightforward matter of determining  $p_{min}$ . The above-mentioned effects can result in significant deviations from Equation (38), which should always be kept in mind. Nonetheless, Equation (38) has its merit for the pump designer and the application engineer/pump user.

$NPSH_R < NPSH_A < NPSH_i$ —Since one generally will have that  $NPSH_R < NPSH_A < NPSH_i$ —that is  $NPSH_A$  is usually less than  $NPSH_i$  but enough to prevent head/performance breakdown—the question arises: “How much cavitation and subsequent cavitation damage will occur under such a situation.” This requires the cavity bubble length to be known, and to that end a first evaluation would be to determine the region where the local (static) pressure drops below the vapor pressure (i.e.,  $p < p_v$ ). Clearly, this is physically unrealistic, but can be evaluated for a single phase flow (numerical simulation). It will provide an indication of the cavitation area and may assist in determining a first approximation of cavity bubble length.

The key to determine the region  $p < p_v$  lies in plotting an isotomic surface for a threshold value  $p_v^*$  at the post-processing stage of a CFD run. With reference to Figure 13, and using the principle of superposition as before, it follows that:

$$p_v^* = p_v + (p_1 - p_{1,i}) \quad (39)$$

where  $p_1$  is the upstream static (suction) pressure of the CFD run, and  $p_{1,i}$  is upstream static (suction) pressure corresponding to the actual  $NPSH_A$ . Then, substituting:

$$p_{1,i} = \rho g NPSH_A - \frac{1}{2} \rho C_1^2 + p_v \quad (40)$$

in Equation (39) one arrives at:

$$p_v^* = p_{01} - NPSP_A \quad (41)$$

with  $NPSP_A = \rho g NPSH_A$  being the available net positive suction pressure.

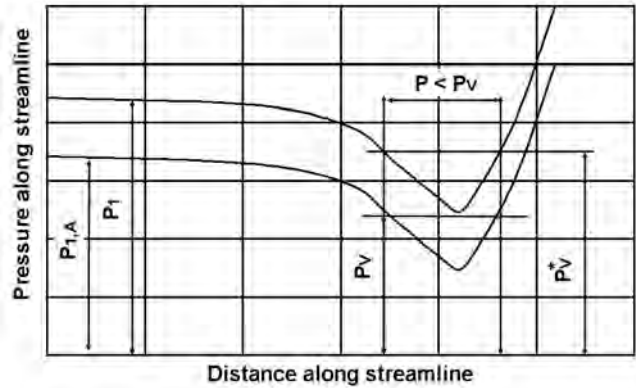


Figure 13. Threshold Value  $p_v^*$  to Determine  $p < p_v$  Region.

From the threshold value  $p_v^*$ , computed by Equation (41), the region  $p < p_v$  is determined/visualized during post-processing after the CFD run. The value used for  $p_1$  (or  $p_{01}$ ) in the CFD run is insignificant in this context, since the flow is driven by pressure gradients.

Figure 14 gives an exemplary outcome of the above-given argumentation. Looking into the impeller eye, it shows the isotomic plot of the region  $p < p_v$ , which is located on the suction side of the impeller blade. The region  $p < p_v$  starts a little distance after the blade leading edge, and has longest streamwise length near the impeller shroud. From a plot like Figure 11 one can obtain an indication of the cavity bubble length to be expected for that particular flow situation. The author has experienced that for low specific speed designs (say, 800 to 1350  $N_q$ ) one can expect that the cavity extends up to about three times the length of the region  $p < p_v$ . Using this information, i.e.,  $L_{cav} \approx 3 L_{p < p_v}$ , one has already a means to evaluate the cavitation erosion potential employing for instance Gülich's correlation (9), or Equation (11).

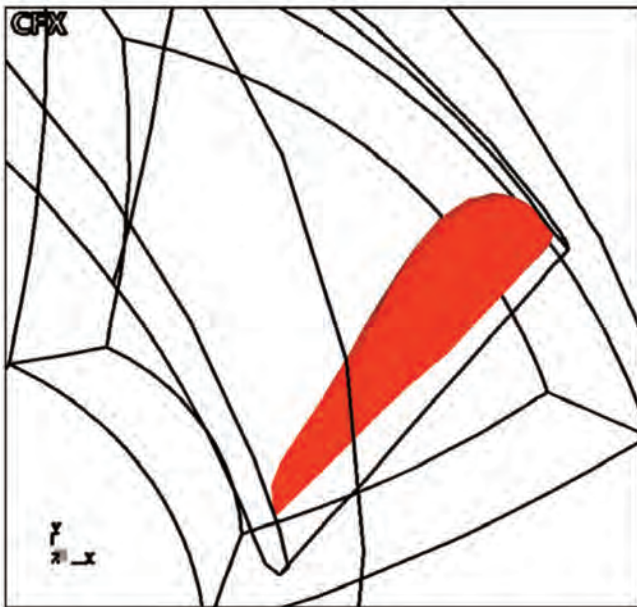


Figure 14. Plot of  $p < p_v$  Region on the Suction Side of an Impeller Blade;  $NPSH_A = 15.5$  m,  $NPSH_i = 28$  m,  $N = 2980$  RPM,  $Q = 400$  m<sup>3</sup>/h.

**Bubble length from cavitation model**—The last few years (commercial) CFD codes have been furnished with cavitation models, enabling simulation of two-phase cavitating flows, which can be used to predict cavitation bubble length and pump (head) performance when  $NPSH_A < NPSH_i$ . The models that have been

developed can be classified as density effect models on the one hand, and bubble dynamic models on the other hand.

Although they are somewhat simplistic, density effect models are attractive since they can be used in single phase codes. They simulate the void of the cavity through a change in density for regions where  $p < p_v$ . Initially, this will be a region like plotted in Figure 11, which gradually expands (primarily downstream) during the (iterative) solution stage of the governing (Navier-Stokes) flow equations. Examples of such models are:

- The ones using a barotropic law, in which density is a prescribed function of pressure only, i.e.,  $\rho = \rho(p)$ , or
- The constant enthalpy of vaporization (CEV) model, in which the vaporization and condensation of the cavitation process is captured from an isenthalpic change of state.

Bubble dynamic models employ a truncated form, or first order approximation, of the Rayleigh-Plesset equation; see for instance Brennen (1994, 1995) or Franc and Michel (2004) for details and in-depth discussion on the Rayleigh-Plesset equation. Bubble dynamic models are closer to reality, but are also mathematically and numerically more complicated than density effect models. They are also more central processing unit (CPU)-expensive. An example of a bubble dynamic model is the volume-of-fluid (VOF) model.

Figure 15 shows an example of a cavity sheet computed with the CEV-model. It visualizes the same situation as Figure 14, but then with the cavitation model enabled. Comparing this plot with Figure 14 it is clearly seen that the length of the cavity is a multiple of the  $p < p_v$  region.

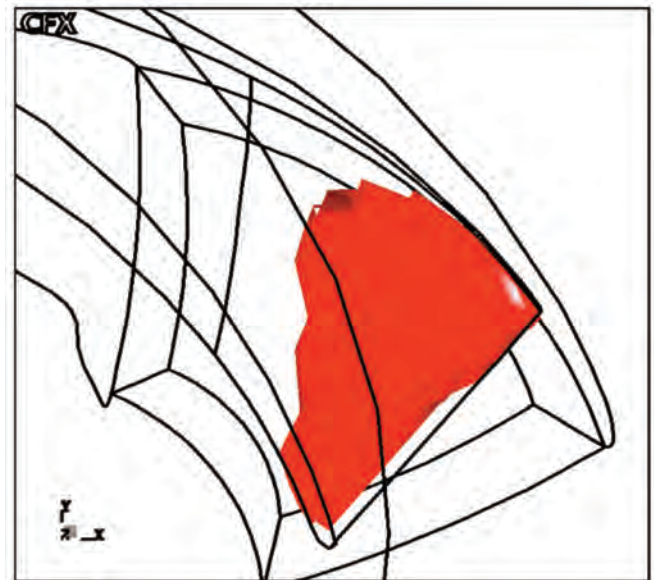


Figure 15. Plot of a Sheet Cavity on the Suction Side of an Impeller Blade, Computed with CEV-Model to Simulate Cavitation;  $NPSH_A = 15.5$  m,  $NPSH_i = 28$  m,  $N = 2980$  RPM,  $Q = 400$  m<sup>3</sup>/h.

The cavitation models currently available can assist the pump designer in evaluating and optimizing impeller designs. It is a numerical analysis tool that enables prediction of:

- Cavity bubble length, and
- $NPSH_R$  associated with a certain head breakdown,

prior to actually building and testing a pump.

Figures 16 and 17 present an exemplary result of employing CFD with CEV-model to simulate cavitation. The graphs show a CFD computed head drop curve (Figure 16) and the  $NPSH_R$  (3 percent) for a centrifugal pump impeller (Figure 17)—both compared to measurements.

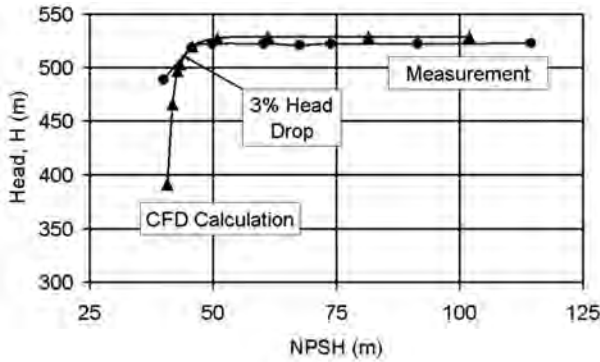


Figure 16. Head Drop Curve from CFD Calculation Using CEV-Model (▲), Compared to Measurement (●). (Courtesy of Visser, 2001)

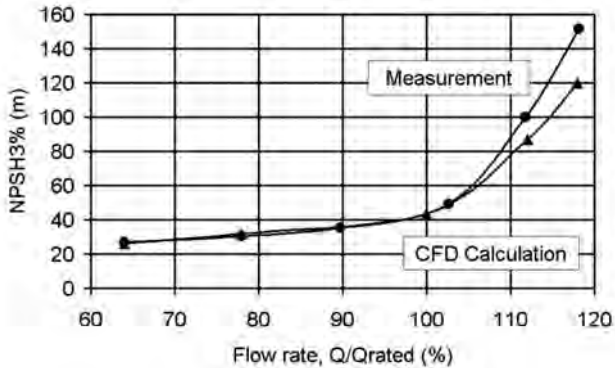


Figure 17. NPSH<sub>3%</sub> from CFD Calculation Using CEV-Model (▲), Compared to Measurement (●). (Courtesy of Visser, 2001)

**NPSHR CRITERIA—EXPERIMENTAL FACTS**

*Cavitation Inception—  
Detection and Physical Peculiarities*

Traditionally cavitation in pumps has been associated with performance deterioration, namely pump head. The condition of suction pressure leading to a certain percent of head drop has been used for many decades in the pump industry to identify the cavitation. Conventionally a 3 percent head drop has been agreed as the index for measuring the cavitation amount and develop cavitation related curves. The total head margin above the vapor pressure at the measuring station (upstream of pump suction flange and away from the impeller blade inlet where cavitation actually occurs) corresponding to such condition was named net positive suction head. Also it was indicated in the standards (exact historical date is unknown) as NPSHR, where R stands for required. Clearly under such condition cavitation is well developed to the point that it produces a drop of head (and efficiency, capacity, power as shown by all shop test data). Therefore the corresponding term “R” should have been always linked with the corresponding 3 percent index and used a more correct symbol such as NPSR3%.

On the opposite side it became very diffused understanding that the term R means a condition for avoiding cavitation at all, i.e., the index NPSHR was and is commonly interpreted as NPSH required to prevent cavitation. Then as logical corollarium the criterion of establishing values of net suction pressure onsite (called NPSHA, A = available) only slightly above the NPSHR (as above defined) was fully considered as a safe condition to prevent cavitation at all. At least this understanding was widely diffused among pump users, system designers (particularly), and even pump vendors.

Moreover the above criterion of NPSHR led the pump designer and user to develop new designs aimed at lowering such values (and so pushing the S-values), ignoring other effects associated with the true physics of cavitation phenomena.

Clearer insights have been obtained by looking at the early inception of cavitation, which has been investigated by using different experimental methods.

*Head Loss Criterion*

A head loss criterion was used back in 1941 in a landmark paper about pump cavitation (Gongwer, 1941) to characterize the pump performance deterioration from early cavitation stage down to large head drop. In Figure 18 (directly scanned from the original paper, as done for several other figures presented in the following sections) a dimensionless cavitation plot is presented, using nondimensional indexes,  $C_2$  (related to capacity) and  $C_3$  (related to  $H_{sv}$  or NPSH). The criterion for head loss corresponds to various percent (0.5, 1.0, 100) of the head parameter  $(2U_{eye})^2/2g$ , i.e., associated with kinetic head of impeller eye peripheral velocity  $U_{eye}$ . The author explains this choice with the argument that cavitation occurs at impeller inlet and is mainly affected by the inlet geometry, while should not be related to full pump head (the experimental investigation included a series of tests with impeller trims). In Figure 18 the top curve for 0.5 percent head loss is indicative of an early cavitation stage. A key peculiarity is the presence of a peak at part capacity (below the shockless value  $C_{20}$ ), which was related by theoretical consideration to a flow instability (Figure 19).

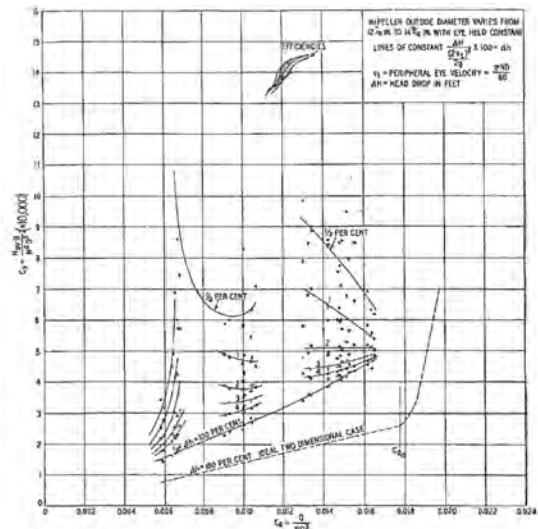


Figure 18. Dimensionless Cavitation Plot (Courtesy of Gongwer, 1941): Peripheral-Flow Index  $C_3$ , Versus Angle of Entry Index  $C_2$ . ( $C_3 = g H_{sv} / N^2 D^2, C_2 = Q / ND^3, H_{sv} = NPSH$  for Head Loss Corresponding to Various Percent (0.5, 1.0, ... 100) of  $(2 U_{eye})^2/2g, D = D_{eye}$ ).

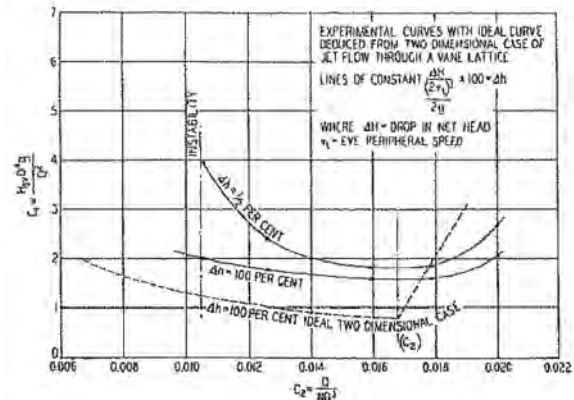


Figure 19. Impeller Cavitation Characteristics (Courtesy of Gongwer, 1941): Through-Flow Index,  $C_1$ , Versus Angle of Entry Index  $C_2$ , ( $C_1 = g H_{sv} D^4 / Q^2$ ).

Although indicative the method of head loss (like 0.0 percent) is not fully accurate for detecting the true inception of cavitation.

*Visual Inception*

Another landmark cavitation paper (Minami, et al., 1960) presented an experimental investigation about cavitation using a transparent pump model and flow visualization by means of stroboscopic light. In Figure 20 (scanned from the original paper) three different criteria are used for characterizing various levels of cavitation through the corresponding net suction head ( $H_{sv}$ ):

- Visual inception at the appearance of first small vapor bubbles on the blade ( $H_{svi}$ ),
- A fixed percent for head drop ( $H_{svd}$ ), and
- Full head breakdown ( $H_{svl}$ ).

Essentially these three cavitation indexes correspond to three different NPSHR criteria, being  $H_{sv} = \text{NPSH}$  and  $R$  required for:

- Inception,
- Head drop,
- Head breakdown.

Moreover with a second x-axis are shown the incidence angles, which are the angles between the blade inlet and the relative flow velocity along a streamline. A positive incidence means that the flow angle, which decreases with flow (at constant speed), is flatter than blade angle, which is fixed.

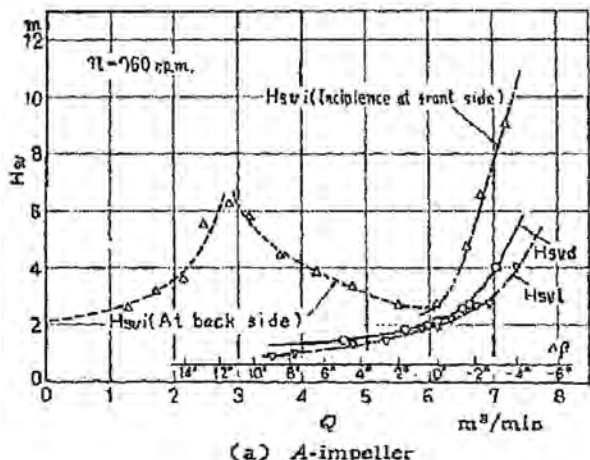


Figure 20. Variation of Required NPSH at Cavitation Limits (from Minami, et al., 1960)—Impeller A ( $D_1 = 7.90$  inch,  $Z = 5$ ,  $\beta_{1b} = 22.20$  Degrees,  $S_1 = 0.24$  inch,  $N_s = 2254$ ).  $H_{svi} = \text{NPSH}_i$  (Visual),  $H_{svd} = \text{NPSH}$  at Percent Head Drop,  $H_{svl} = \text{NPSH}$  at Head Breakdown. Front Side is Pressure Side (PS), Back Side is Suction Side (SS). Shockless Capacity is at  $\Delta\beta$  (Incidence Angle) = 0.0 Degrees.

Figure 21 gives the experimental evidence of the following cavitation aspects:

- The visual inception curve has a peculiar V-shape with a minimum and a peak (at reduced flow). Moreover visual cavitation appears on the blade either on the front side (called PS = pressure sided by the paper authors) or on the back side (called SS = suction side).
- The minimum value for  $H_{svi}$  (or  $\text{NPSHR}_{\text{vis-inc}}$ ) is at zero incidence angle, and corresponding capacity is called shockless capacity ( $Q_{sl}$ ) or best cavitation point.
- The curves for given head drop and head breakdown are continuously decreasing from high to low flow. The trend at part flow ( $Q < Q_{sl}$ ) does not reflect at all the inception curve.

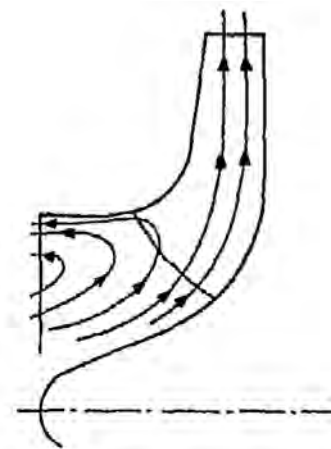


Figure 21. Flow Pattern at Partial Capacities (from Minami et al., 1960). Backflow (Suction Recirculation) Starts below Critical Capacity Coincident with Peak of  $H_{svi}$  ( $\text{NPSH}_i$ ).

Visual observations (Minami, et al., 1960) showed a flow instability on the blade at the occurrence of the  $H_{svi}$  - peak. Then additional investigation was performed by making flow traverses at the impeller inlet with a Pitot tube. It was found that below the peak capacity the inlet flow pattern presented both a backflow (Figure 21) along with a swirling flow. The  $H_{svi}$  - peak was occurring for all the impellers at the onset of this peculiar flow pattern (which later was called in the pump industry suction recirculation). All the above characteristic aspects were found with other three impellers, as shown in Figure 22.

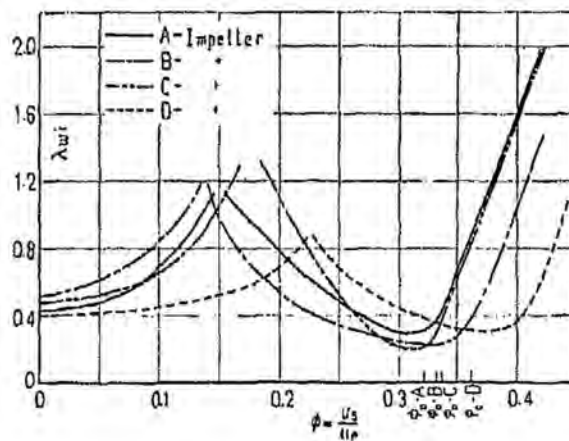


Figure 22. Coefficient of Pressure Drop at Tip Leading Edge Versus Capacity (Inlet Flow Coefficient) at Visual Cavitation Inception. (Courtesy of Minami, et al., 1960)

The use of flow visualization for cavitation characterization was limited to special pump applications in the 60s (Wood, et al., 1960; Wood, 1963). It was applied in the 70s in Europe to support the design of modern reactor feed pumps for nuclear power plants (Grist, 1974) or to solve some field cavitation damage problems with boiler feed pumps (Dernedde and Stech, 1982; Florjancic, 1982). Thereafter it was more widely used for solving field problems (Schiavello, 1986) and research (Gulich and Pace, 1986; Cooper, et al., 1991; Hergt, 1991).

*Acoustic Inception*

Another powerful experimental method for detecting the cavitation inception is looking at high frequency cavitation noise with hydrophones (miniature piezoelectric pressure transducers flush mounted at pump suction). Figure 23 presents a typical high

frequency signal at selected frequency of 40 kHz, measured at constant capacity ( $Q/Q_{bep} = 1.0$ ) and constant speed with decreasing NPSE (net positive suction energy, i.e., using energy instead of head as index for suction condition of pressure and velocity). Also the NPSE curve corresponding to the energy head drop criterion is shown. The test pump with a Plexiglas® window at inlet allowed the visual cavitation inception (at point B in Figure 23). The acoustic inception is given by the sharp increase of the noise signal, i.e., very close to point B. With further reduction of suction pressure the cavitation and noise continue to rise reaching a maximum after which the noise first drops and then increases again (at full performance breakdown). There is strong evidence that the peak noise corresponds to the point of maximum erosion, while the performance (energy or head) is still unaffected (0.0 percent drop). The drop of noise beyond such point when cavitation becomes more extensive is likely associated with absorption of sounds by presence of large vapor pockets (cushioning effect). Noise signals for other high frequencies were similar to the one for 40 kHz.

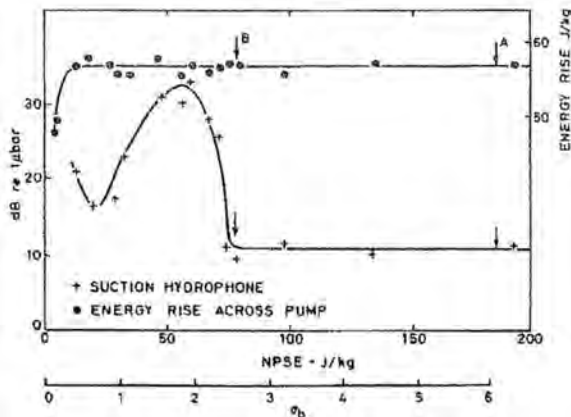


Figure 23. Typical High Frequency Noise Output as NPSE Is Varied at Constant Flow and Speed (Courtesy of McNulty and Pearsall, 1979, 1982). Signal Frequency: 40 kHz,  $Q/Q_{bep} = 1.0$ , Visual Inception: Point B.

The variation of the acoustic inception point with flowrate is shown in Figure 24, where the blade cavitation number at inception is used as dimensionless parameter for NPSE. It is evident the curve of the acoustic cavitation inception versus capacity has a shape similar to the visual cavitation inception curve, still presenting a minimum (or best cavitation point) at BEP (found close to shockless capacity). Then the cavitation inception method represents another NPSHR criterion. It is worth noticing that such a criterion would give insights about the NPSHR corresponding to maximum erosion damage risk, while an NPSHR criterion based on 0.0 percent head drop could lead to erroneous conclusions (absence or minimal cavitation) with high risk for cavitation damage.

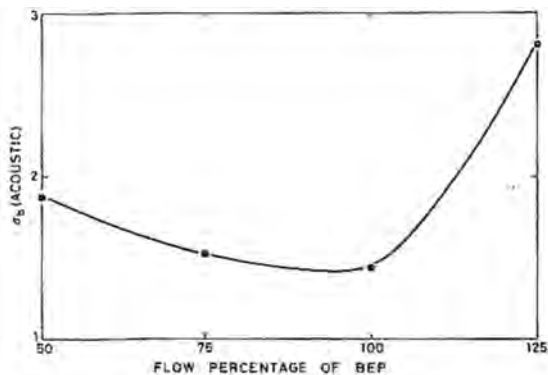


Figure 24. Effect of Flow on Acoustic Inception. (Courtesy of McNulty and Pearsall, 1979, 1982)

#### Additional Methods and Experimental Insights

At the cavitation inception small vapor bubbles are generated that both change the medium physical properties (two-phase flow with drastic impact on compressibility, Young modulus, and so speed of sound), and also the internal flow patterns (especially with increasing cavitation pockets) reflecting higher unsteadiness as suggested by flow visualizations and cavitation noise observation.

Then several methods have been applied for investigating the cavitation behavior from inception down to extensive growth with the scope of:

- Gathering additional experimental insights,
- Investigating simple, economic, and not invasive methods suitable for monitoring/diagnostic tools applicable with actual industrial pumps and field constraints.

The literature is quite wide and very dispersive. Here the basic information is presented with the aim of showing physical principles and limitations of the methods.

A centrifugal laboratory pump with transparent impeller shroud and casing side wall at front was used (Kercan and Schweiger, 1979) for investigating cavitation with several cavitation noise methods in addition to flow visualization and classical techniques of performance deterioration (head, flow, efficiency). The disposition of the various cavitation noise pickups is shown in Figure 25, specifically aimed at detecting:

- Fluid borne noise with low frequency pressure pulsations (pressure transducers P1 and P2, flush mounted at pump suction and discharge, respectively).
- Airborne noise at high frequency (microphones M1 and M2, outside the pump).
- Structure borne noise at high frequency (accelerometers A1, A2, and A3 installed on the suction pipe, outer, and side wall of the spiral casing, respectively).

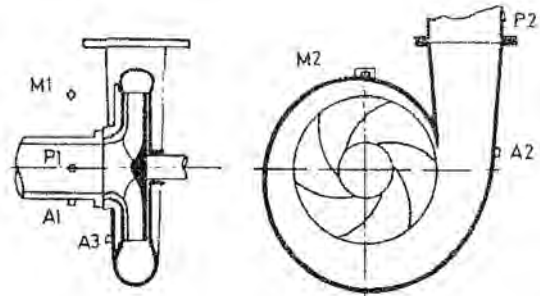


Figure 25. Disposition of Various Cavitation Detection Pickups (Courtesy of Kercan and Schweiger, 1979). Visible Cavitation (Transparent Impeller Shroud and Casing Side Wall at Front), Fluid Borne Noise (Low Frequency Pressure Pulsations: P1, P2), Airborne Noise (High Frequency Microphones: M1, M2), Structure Borne Noise (High Frequency Accelerometers: A1, A2, A3).

The experimental trends of these parameters (expressed in decibels [dB]) versus the dimensionless cavitation coefficient (NPSH referred to  $U_{eye}^2/2g$ ) are shown for the BEP capacity in Figure 26 (airborne noise) and Figure 27 (structure borne noise or vibrations) for various frequencies. All these signals permit to determine an inception cavitation point and also a peak point in terms of NPSH, which are not influenced for each parameter by the selected frequency. However the corresponding  $NPSH_{inc}$  varies for each pickup (i.e., nature of parameter and location of pickup). Also the peak level, which may be associated with highest severity level of cavitation, is strongly dependent from location of pickup (Steller, 1983). This aspect is particularly true for the accelerometers (Figure 27). It should be underlined that the amplitude level of the

response of the accelerometers is influenced by the mechanical characteristics of the casing (material and thickness) through a transfer function that is usually unknown (Okamura, et al., 1985). Therefore the use of accelerometers installed on the pump casing (e.g., volute, bearing frame) can give only relative indications as compared to similar measurements with the same pump casing (e.g., effect of design changes like a different impeller).

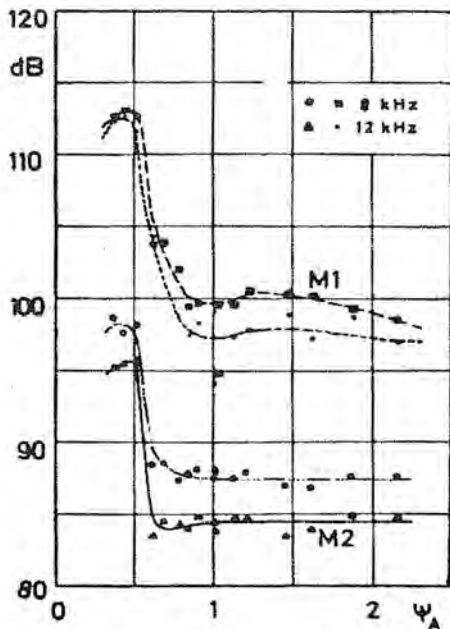


Figure 26. Airborne Noise Level Versus Cavitation Coefficient at Constant Speed and BEP Flow (Courtesy of Kerčan and Schweiger, 1979), (Decibel =  $20 \log P/P_0$ ,  $P_0 = 210^{-5} \text{ N/m}^2$ ).

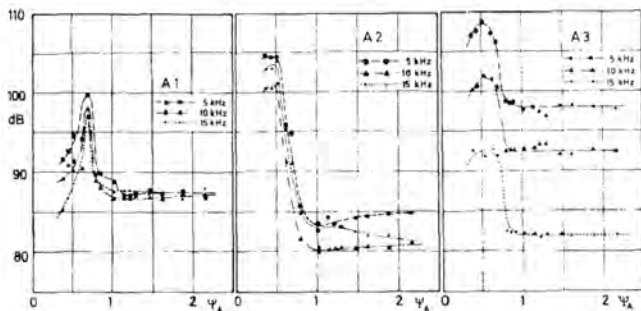


Figure 27. Vibrations (Accelerations) Measurements Results on the Suction Pipe (A), Spiral Casing (B), and the Side Wall of the Spiral Casing (C) at Constant Speed and BEP Flow (Courtesy of Kerčan and Schweiger, 1979). (Decibel: Reference Gravity Acceleration.)

In general these measurements at the present time cannot be used for assessing intensity of cavitation in absolute terms in relation to potential damage. However they can be used for monitoring and also support data for cavitation diagnosis (shop and field situations).

A laboratory mixed-flow pump ( $N_s = 5000 \text{ US}$ ) was used (Schiavello, 1982) to investigate the suction recirculation and its effect on pump performance at part flows, namely the presence of dip in the head curve and also shutoff power. The onset and growth of the suction recirculation were experimentally determined by using flow traverses in the suction pipe with five-holes and also wall static pressure measurements. The critical capacity corresponding to sudden onset of suction recirculation was found at 71 percent of BEP or nominal capacity (same value from probe and static pressure). Moreover traditional NPSH curves were

measured with both 1 percent and 3 percent head drop. The normalized head and efficiency curves (measured with ample NPSHA) and also both NPSHR curves are shown in Figure 28. Several observations can be inferred:

- The onset of suction recirculation is in correspondence of the head dip, which might be produced by the same flow mechanism triggering the recirculation, i.e., flow separation near blade leading edge on the suction side (Schiavello and Sen, 1980, 1981).
- Both the NPSHR curves present a sharp U-shape with a minimum (82 percent  $Q_{\text{bep}}$ ) and a peak at 70 percent  $Q_{\text{bep}}$ , i.e., very close to onset of suction recirculation, confirming other literature data (Minami, et al., 1960).
- In the capacity range with presence of suction recirculation the NPSHR curves decrease from the peak and then rise again. This rise is likely associated with a cavitation mechanism driven by the suction recirculation, which presents increasing intensity toward shutoff as determined from probe measurements.

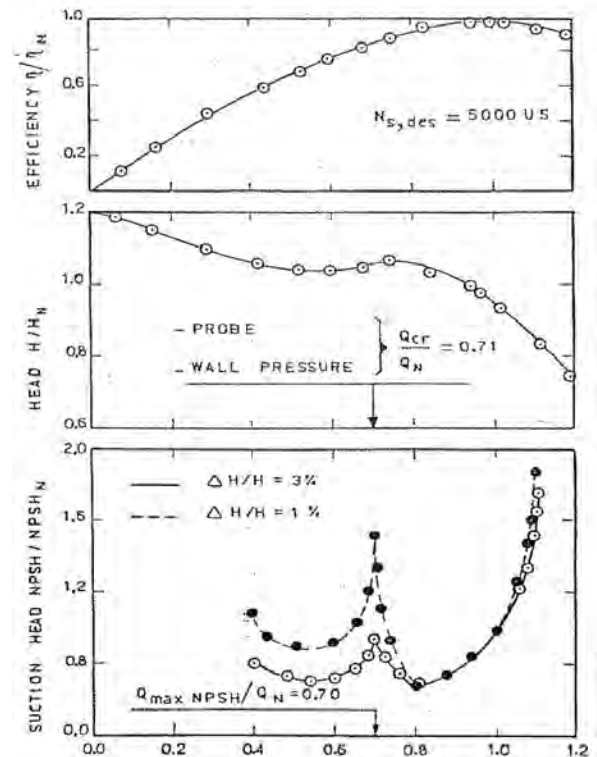


Figure 28. Mixed-Flow Pump Performance: Liaison Between Suction Recirculation Onset Capacity ( $Q_{cr}/Q_N$ ) and NPSH Peak Capacity. (Courtesy of Schiavello, 1982)

The shape of the cavitation inception curve in the full capacity range (from 10 percent up to 130 percent  $Q_{\text{bep}}$ ) was investigated with various indirect methods (Kerčan and Schweiger, 1979) including:

- Head (first discontinuity in the curve),
- Sound level (microphone), pressure pulsations at suction and discharge (flush mounted pressure transducers), casing wall vibrations (accelerometer), and also torque fluctuations (dynamic torsionmeter).

All the corresponding inception curves are shown in Figure 29 (top-to-bottom, respectively). Position of peak around 70 percent BEP is confirmed, with some scatter, plus the inception curves are continuously rising toward shutoff below 60 percent  $Q_{\text{bep}}$  (approximately), i.e., with growing suction recirculation intensity.

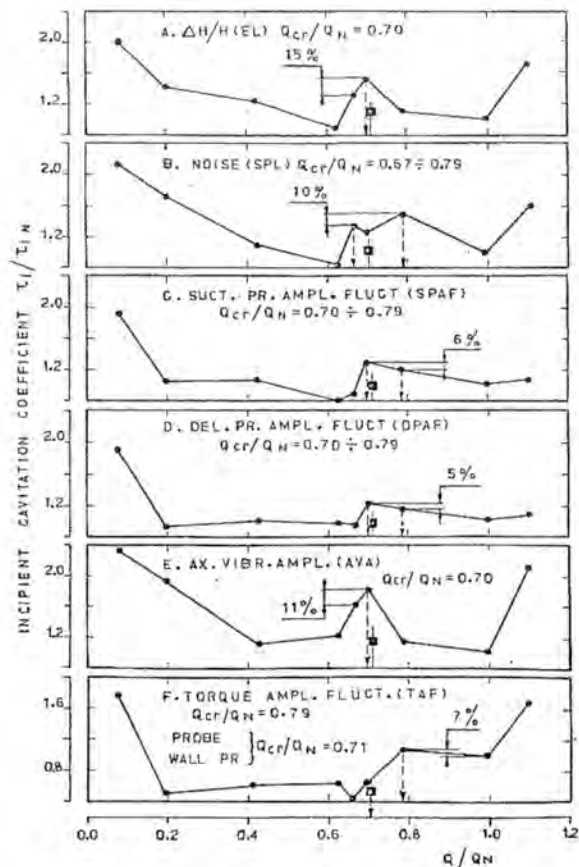


Figure 29. Cavitation Inception Curves in the Whole Capacity Range from Shutoff to Overcapacity Derived with Indirect Experimental Methods. Suction Recirculation Onset Capacity ( $Q_{cr}/Q_N$ ) Directly Detected with Five-Hole Probe and Wall Static Pressure near the Impeller Inlet. (Courtesy of Schiavello, 1982)

Axial flow inducers have been widely investigated mostly in relation to overall cavitation performance and flow instabilities. A thorough laboratory research with an unshrouded inducer of industrial design inside a transparent casing (Boccazzi, et al., 1989) have included cavitation characterization with flow visualization and noise measurements (flush mounted hydrophones in the suction pipe close to blade inlet). The overall amplitude of cavitation noise level (measured as RMS value in a frequency spectrum from 0 Hz up to 20 kHz) versus NPSH at various capacities is shown in Figure 30. All parameters are dimensionless, i.e., undimensional cavitation noise coefficient ( $CNL_u = 2gCNL/U_{tip}^2$ ), cavitation coefficient ( $\sigma_u = 2gNPSH/U_{tip}^2$ ), and flow coefficient ( $\varphi = Q/A U_{tip}$ ). The start of cavitation (acoustic inception) is identified for each curve at the first discontinuity point (i.e., net change in the curve slope). Then the trend of cavitation coefficient versus flow coefficient was determined for various degrees of NPSH level (Figure 31), i.e., from top to bottom: acoustic inception (highest NPSH), visual inception (barely visible bubble length starting at blade leading edge), cavitation bubble with radial depth of 10 and 20 mm (0.4 and 0.8 inch), 3 percent head drop. Basically each curve corresponds to a different NPSHR criterion and presents a different shape evolving from a V-shape (at cavitation inception, acoustic and visual) to the more familiar trend (continuously decreasing with flow) of NPSHR3% head drop. The flow coefficient for zero incidence angle (shockless flow,  $\varphi_{sl} = 0.132$ ), which is marked in Figure 42, is a truly experimental value not a theoretical one (i.e., derived from calculations and drawings of geometrical data), because it was determined from both static pressure measurements on the

casing wall facing the blade tip section and also from relative velocity pattern obtained using a laser Doppler anemometry (LDA) (Boccazzi, et al., 1989). It is fully evident that the minimum NPSH value in the cavitation inception curves, acoustic and visual, is practically occurring at the shockless flow. Visual observation of the cavitation pocket clearly indicated that cavitation was developing on the blade front side (or suction side) for flow below the shockless one (i.e., along the left branch of the V-curve), while it was present on the blade back side (or pressure side) above the shockless flow (right branch of the V-curve). The range of flow coefficient presented varies from 0.103 up to 0.155, i.e., 78 percent up 117 percent of the shockless flow or best cavitation point. Also the onset of suction recirculation was experimentally found at the flow coefficient around 0.103 from visual observation (unstable reversed flow at tip blade leading edge), static pressure data, and velocity pattern obtained with the LDA.

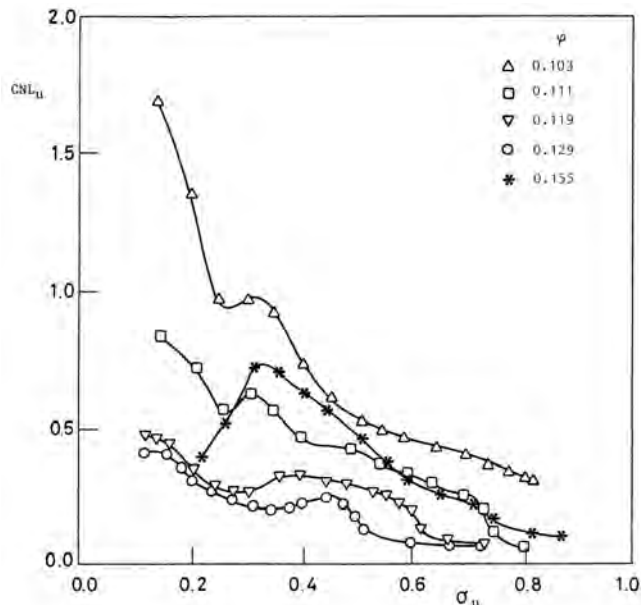


Figure 30. Nondimensional Cavitation Noise Level Versus Cavitation Coefficient (Courtesy of Boccazzi, et al., 1989) ( $\sigma_u = 2 g NPSH / U_{tip}^2$ ,  $CNL_u = 2 g CNL / U_{tip}^2$ ).

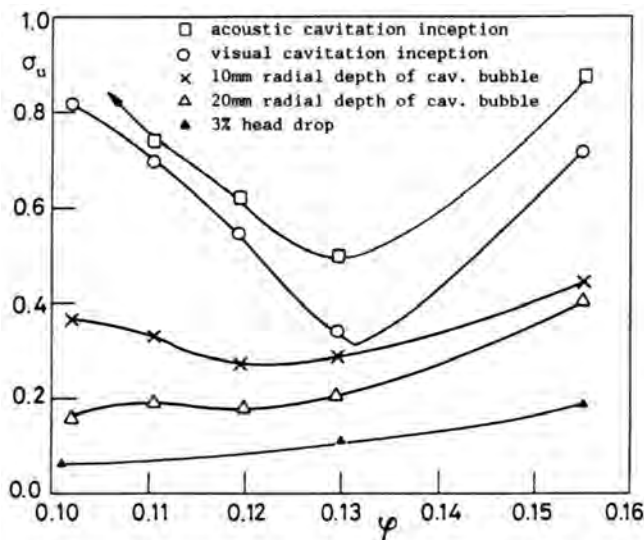


Figure 31. Cavitation Coefficient Versus Flow Coefficient at Various Cavitation Levels (From Top: Acoustic Inception, Visual Inception, Cavitation Bubble with Radial Depth of 10 and 20 mm, 3 Percent Head Drop). (Courtesy of Boccazzi, et al., 1989)

Some frequency spectra of cavitation noise level (in dB) are shown in Figure 32 for various NPSH level (same as in Figure 42) decreasing from top to bottom row and three peculiar flow coefficients, i.e., maximum, shockless, and minimum at suction recirculation from the left to the right column, respectively. It is evident how the frequency content expands with growing cavitation intensity, with significative and increasing presence in the ultrasonic range (above 10 kHz), i.e., not audible cavitation noise.

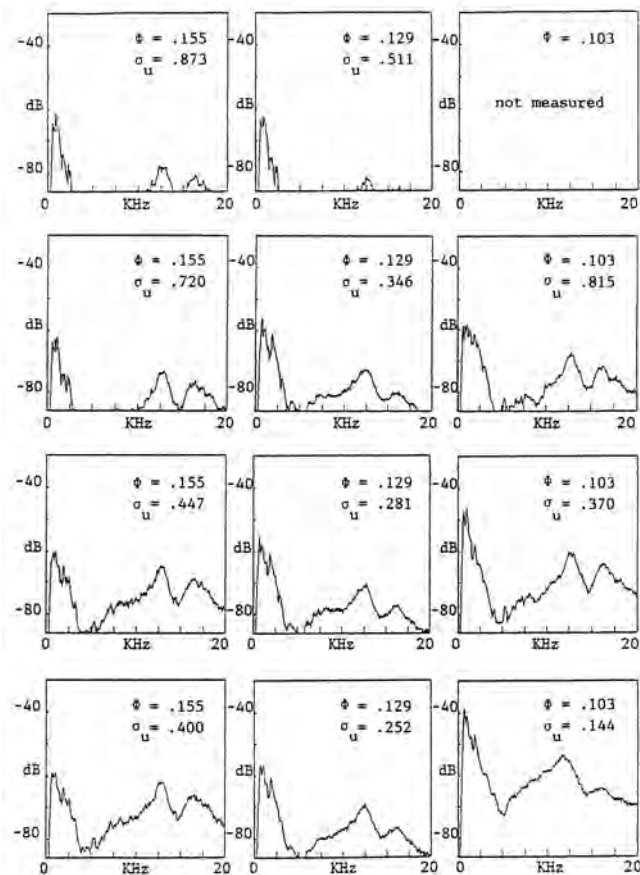


Figure 32. Frequency Spectra of the Suction Pressure Pulsations for: Acoustic Inception (Row 1), Visual Inception (Row 2, Radial Depth of Cavitation Bubble of 10 mm (Row 3), and 20 mm (Row 4). (Courtesy of Boccazzi, et al., 1989)

#### NPSHR Criteria—Key Remarks

All the above experimental data clearly indicate that there are several cavitation effects and in principle different NPSHR could be adopted to characterize such effects or various levels of cavitation intensity, namely:

- Performance Impairment (head, efficiency).
- Metal damage (life reduction).
- Noise: audible (up to 10 kHz. Not necessarily implying damage), ultrasonic (10 to 200 kHz plus. Likely causing damage).
- Pressure pulsations.
- Torque fluctuations.
- Casing vibrations.
- Bearing housing vibrations.

Moreover laboratory observations with model pumps, shop test data with actual industrial pumps, and also field experience particularly concerning cavitation damage suggest the following key remarks:

- Cavitation is related to pressure field.
- All above effects having potential impact on pump reliability and life are linked with pressure.
- Head degradation is only one side effect with no univocal liaison with reliability and even hiding the most risk situation.
- Cavitation requirement criteria linked to head (like: net positive suction head or NPSHR for whatever percent of head drop) are weak and not fully representative of the cavitation physics.
- Cavitation requirement criteria should explicitly include pressure to reflect the true physics.

#### NPSHA MARGINS—KEY FACTORS

##### Cavitation Modes

##### Blade Attached (or Sheet) Cavitation

The cavitation visualization studies (Minami, et al., 1960; Boccazzi, et al., 1989) permit determination of the curve of the NPSH at the condition of visual inception (visible appearance of first small vapor bubble) versus the pump capacity. As shown above, this curve had a very peculiar shape like a V (U)-shape. The NPSH<sub>i</sub> (i = inception) has a minimum at a capacity that corresponds to shockless inlet flow (Q<sub>sl</sub>), i.e., the relative flow reaches the blade leading edge with an incidence angle around zero degrees. It is important underlining that the shockless capacity is not necessarily coincident with the pump BEP capacity and also it does not change with impeller trimming, which shifts the BEP capacity to smaller values. The NPSH<sub>i</sub> increases at Q > Q<sub>sl</sub> and Q < Q<sub>sl</sub>, with cavitation starting on the pressure (hidden) and suction (visible) side of the blade, respectively. At part flow, the NPSH<sub>i</sub> peaks at capacity slightly higher than the critical suction recirculation onset capacity, Q<sub>rs</sub> (rs—suction recirculation) (Minami, et al., 1960; Schiavello, 1982). The peak of NPSH<sub>i</sub> is attributed to a critical incidence angle causing flow separation (Gongwer, 1941) or stalling incidence (Schiavello and Sen, 1980, 1981).

It is worth noticing that the increase of the cavitation inception curve at Q > Q<sub>sl</sub> and Q < Q<sub>sl</sub> is primarily caused by a quick increase of the relative velocity and a consequent pressure drop near the leading edge (Gulich, 2001), which is followed by a pressure recovery (Boccazzi, et al., 1989), i.e., the cavitation is not due to a shock loss as commonly thought. This pressure drop moves around the blade inlet from the pressure side (Q > Q<sub>sl</sub>) to the suction side (Q < Q<sub>sl</sub>) as suggested by basic flow insights (Dernedde and Stech, 1982) and confirmed by CFD studies (Visser, 2001).

At the point of the visual cavitation inception, the rate of the erosion damage is practically zero. A cavitation vapor pocket with increasing length develops if the suction pressure, or NPSH, is continuously decreased, like during test of head decay at constant rotational speed and constant capacity (Figure 2). Pumps in the field operate with NPSHA (A = available) higher than the conventional NPSHR, but significantly below the NPSH<sub>i</sub>, and so a certain amount of cavitation is present.

In order to produce damage, the vapor bubbles must collapse in the vicinity of the metal surface. Normally, it occurs for the regime characterized in the literature as blade attached (or sheet) cavitation, which is more common in the usual capacity operating range. In this cavitation mode, the curve of the cavitation erosion rate (ER = MDP/Time, where MDP = mean depth penetration versus capacity at constant speed/NPSHA (Grist, 1974) has a peculiar V-shape, with the minimum at the shockless capacity (Figure 33), which is similar to the NPSH<sub>i</sub> curve. As shown in Figure 34 the damage develops like pitting (spongy appearance) on the blade pressure (hidden) side for flowrates above the shockless capacity. Usually there is an audible crackling noise like the sound produced by gravel unloading. At flowrates below the shockless one, the cavitation damage occurs on the suction (visible) side of the vane

still like pitting as evident in Figure 35. This cavitation is not necessarily audible, being characterized with ultrasonic frequency content. It is worth noticing that the damage curve is significantly steeper for  $Q > Q_{s1}$  denoting more severe cavitation in terms of damage for pressure side cavitation in the regime of blade attached cavitation.

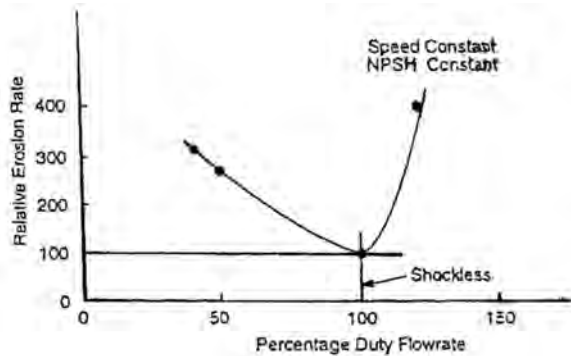


Figure 33. Variation of Erosion Rate with Capacity with Blade Attached Cavitation Mode. (Courtesy of Grist, 1974).

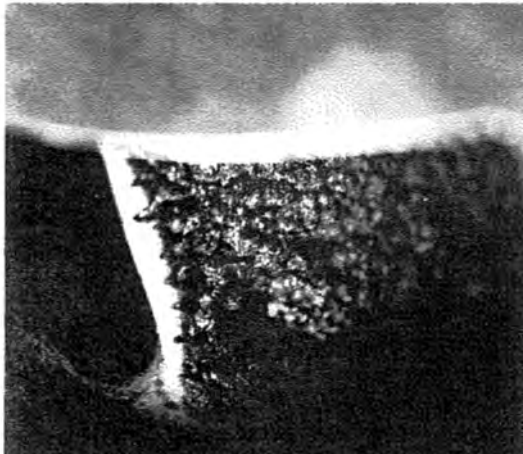


Figure 34. Cavitation Damage on Pressure Side (Back or Hidden) of Impeller Blade. (Courtesy of Cooper and Antunes, 1982)



Figure 35. Cavitation Damage on Suction Side (Front or Visible) of Impeller Blade. (Courtesy of Cooper and Antunes, 1982)

*Cavitation Induced by Suction Recirculation (Vortex Cavitation)*

Visual observations with stroboscopic light show that the cavitation bubble on the blade suction side becomes more and more unstable as the capacity is continuously decreased below the suction recirculation point toward shutoff. The cavitating bubble clouds separate from the blade suction surface and move into the blade channel. Essentially a new flow regime takes place that is characterized by “Strongly intermittent cavitation-suction

recirculation” (Schiavello, 1986). As a generic indication, such very unsteady flow regime occurs in the capacity range from zero percent to an upper capacity, which is smaller or closer to the suction recirculation onset capacity,  $Q_{rs}$ , depending on impeller design,  $U_{eye}$ , and NPSHA level.

Experimental investigation by means of a high speed movie camera along with stroboscope (Okamura and Miyashiro, 1978) clearly shows that at low flowrate two different patterns of cavitation, sheet cavitation and vortex cavitation, occurred alternatively near the leading edge of the impeller blades, as schematically shown in Figure 36. The cavitation started on the blade suction surface far away from the leading edge, moved upstream with an abrupt stroke, and collapsed on the pressure surface of the next blade. This cavitation called vortex cavitation is attributed to the impeller suction recirculation. In fact, a vortex is generated by the shear forces at the interface between the reverse flow leaving the impeller near the front shroud, and the ordinary forward flow entering into the impeller near the hub, as shown in Figure 37(a). Moreover, streams of both backward and forward flow also can be suspected to occur in the blade-to-blade plane in the inlet region of the blade channel, as sketched in Figure 37(b). Then, shear force components also exist in this plane and contribute to the generation of a complex vortex in the three-dimensional space. When the inlet pressure (therefore NPSHA) is low enough and also the strength of the vortex (i.e., intensity of the suction recirculation) is high enough, the pressure in the vortex core drops below the saturation pressure and cavitation conditions are reached. A filament of cavitating flow develops, starting on the suction side of the blade and ending on the pressure side of the next blade, as shown in Figure 37(c). This vortex oscillates in a direction normal to the blade surface, i.e., more or less in the direction of the main flow, as sketched in Figure 37(d).

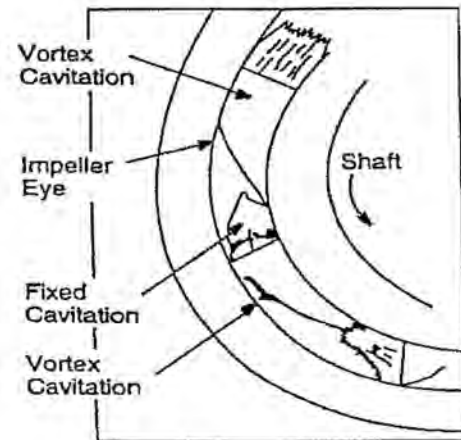


Figure 36. Alternating Sheet Cavitation with Vortex Cavitation. (Courtesy of Okamura and Miyashiro, 1978)

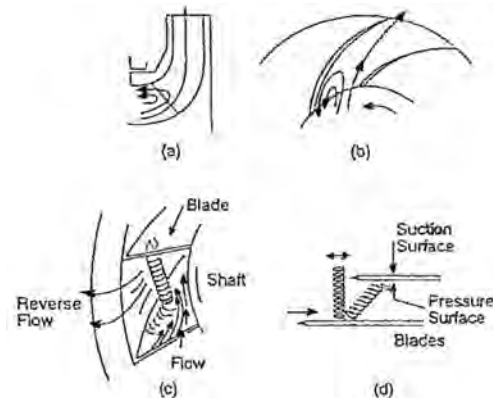


Figure 37. Suction Recirculation (a-b) as Source of Vortex Cavitation (c-d). (Courtesy of Okamura and Miyashiro, 1978)

Consequently, damage is typically caused in the form of a single large crater at the midspan of the blade on the pressure (hidden) side. The crater is surrounded by a zone with irregular pitting and can even perforate the blade (Figure 38, photo made after cutting a large specimen from the blade) even producing the breakage of a blade portion. This is shown in Figure 39, which also presents the appearance of the suction side of the blade, where the hole borders have a net contour, without marked pitting in the surrounding zone. Also this aspect of the suction side (absence of cavitation damage) is a typical sign of the vortex cavitation mode driven by the suction recirculation. Typically an intermittent noise like flashing is observed with the vortex cavitation. The field damage shown in Figures 38 and 39 was experienced in the first stage impeller of a four-stage pump, which was operating for 600 hours with the following conditions:  $Q_{duty}/Q_{rs} = 0.88$  ( $Q_{rs}$  is predicted with empirical correlation),  $Q_{duty}/Q_{bep} = 0.77$  ( $Q_{bep}$  is basically given by the additional stages),  $Q_{duty}/Q_{sl} = 0.63$  ( $Q_{sl}$  is for the first stage impeller),  $NPSHA/NPSHR = 1.30$ . The impeller was clearly oversized and the NPSHA margin above NPSHR was apparently adequate based on common practice, but actually too low as the NPSHA was much below  $NPSH_i$ .



Figure 38. Aspect of Blade Surface under Direct Attack of Vortex Cavitation from Suction Recirculation. Cavitation Damage on the Pressure Side as a Large Crater Surrounded by Irregular Pitting.



Figure 39. Blade Breakage Caused by Vortex Cavitation from Suction Recirculation (Operating Time: 525 Hours, Impeller Material: CF3M). Hole with Net Contour Produced from Vortex Acting on Backside.

The trend of the  $NPSH_i$  curve versus capacity for the vortex cavitation mode and therefore in presence of suction recirculation is not well known due to lack of experimental data and total absence of theoretical prediction models. However it can be inferred that the  $NPSH_i$  is rising as the capacity is reduced toward shutoff, following the increasing strength of the suction recirculation (driving mechanism), as supported by the indirect measurements shown in Figure 29.

A typical curve of  $NPSH_d$  ( $d =$  damage) that can produce significant erosion damage throughout the whole range of operations is shown in Figure 40 as it reasonably follows the shape of the  $NPSH_i$  curve for both main cavitation modes discussed above. The  $NPSH_d$  is not unique and depends upon the various factors as discussed later. Moreover a typical curve for the conventional NPSHR (at 3 percent head drop) is presented in Figure 40, which basically gives the qualitative map defining key cavitation aspects, effects, and location, also in relation to basic hydraulic design parameters ( $Q_{sl}$ , incidence angle,  $Q_{rs}$ ). This cavitation map should be kept in mind for the pump design and cavitation field problem diagnosis.

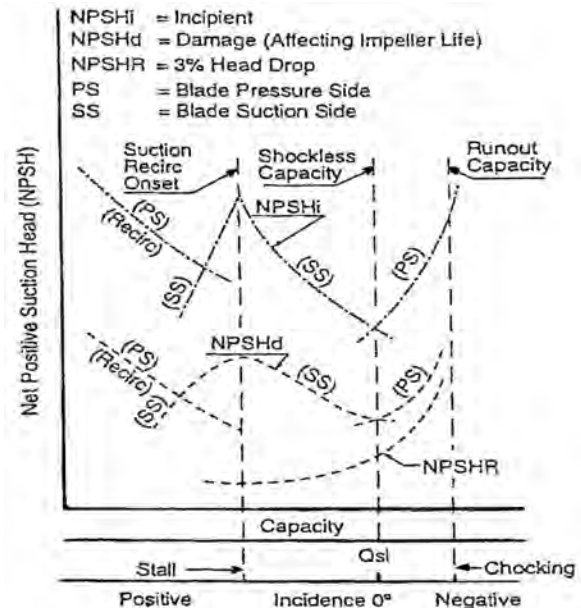


Figure 40. NPSH—Peculiar Curves Defining Various Cavitation Modes. (Courtesy of Schiavello 1992, 1993, Turbomachinery Laboratory)

#### Cavitation Due to Secondary Flows at Blade Fillets (Corner Vortex)

In many cases, cavitation damage has been found at the fillet between the blade suction side and the impeller hub surface. The damage appears to be caused by a strong vortex, which is confined in the blade root-to-hub corner and generates a drilling action leading to rapid perforation of the impeller hub, and in many cases to shaft damage (Figure 41). The flow sources of such corner vortex are the intense shear forces associated with the secondary flow patterns due to the interaction of the blade surface velocity profile and the boundary layers of the impeller hub surface. Flow separation may be a contributory source, but not necessarily.



Figure 41. Cavitation Damage Combined from Sheet Cavitation (Suction Side) and Corner Cavitation.

### *Cavitation Inside Vaned Diffuser (or Volute)*

Cavitation has been observed inside the blade passage of a vaned diffuser (Gülich, 1987) presenting distinct aspects, which can be associated to different flow sources leading to cavitation:

- Large cavitation pocket visible (with transparent diffuser) on the blade pressure side (facing the throat), which appeared as thick sheet cavitation partially choking the throat and causing large head drop at runout capacity, i.e., very high flowrate above the BEP capacity (Scott and Ward, 1992).
- Cavitation damage like pitting in a circular zone located on the side wall and closer to the diffuser exit. The deepest pits were situated in the central area, which appeared caused by a vortex cavitation normal to the wall and caused by flow separation (Cooper and Antunes, 1982).
- Cavitation damage at the diffuser inlet on the suction side (facing the impeller) of the vanes and also on the two annular wall surfaces facing the outer edge of the impeller shrouds. Moreover the damage might be present at the impeller exit, both on the vane pressure side (visible by looking at the impeller outlet periphery) for the full vane span, and also around the external edge of the front-rear shroud. The damage aspect is characterized by uniformly spread pitting with many and nearly identical microraters. This suggests a cavitation erosion mechanism with a cluster of thousands of small vapor bubbles, homogeneously distributed and individually imploding. The flow source of such cavitation mechanism is related to pressure pulsations with very high amplitude such to produce instantaneous pressure peaks below the vapor pressure. This cavitation mode can be referred as unsteady cavitation, due to impeller-diffuser interaction.
- Cavitation damage like fine pitting on the blade suction side. However the damage pattern is very peculiar being present only on one circular sector of the diffuser, i.e., affecting only a few adjacent vanes. This asymmetric damage pattern has been observed in the first stage diffuser of multistage feedwater pumps for fossil power plants and also the diffuser of a single-stage reactor feed pump for nuclear power plants. The flow source of such peculiar asymmetric cavitation is seemingly related with a flow distortion, which is presently explained with different and conflicting theories.

Some of the above cavitation phenomena have been also observed inside volute passages near the throat. It is well-known that at very high flow rates (130 percent  $Q_{bep}$  or more, depending on throat size and impeller head) cavitation occurs in the volute throat leading to high-full head drop).

### *Inlet Flow Influence*

*Flow distortion*—A strong flow influence on cavitation inception ( $NPSH_i$ ) and damage ( $NPSH_d$ ) is produced by the flow distortion at the impeller eye, as induced by the upstream geometry, i.e., inlet chamber and/or suction piping.

For side suction pumps the shape of the  $NPSH_i$  curve can be highly altered by the suction casing, which tends to displace and smooth the minimum and the peak. The degree of distortion becomes stronger with increasing capacity. Visual observations clearly show (Schiavello, 1986) that both the shape and size of the cavitation bubble on each impeller blade change periodically with time, as the blade crosses flow zones with either positive or negative swirling velocity component relative to the impeller rotation and causing less intense or more severe cavitation, respectively. This kind of flow distortion can lead to higher pressure pulsations, pump vibrations, and possibly cavitation damage.

Moreover a possible flow distortion caused by a side suction casing is negatively affecting the conventional NPSHR curve (3 percent). Proven design criteria exist today for improving the flow pattern in the side suction casing and producing a nearly uniform flow at the impeller eye by using guide vanes with optimized

shape. One key effect is a lower NPSHR with higher improvement at higher flowrates (Bunjes and Op De Woerd, 1984). Consequently the suction specific speed is markedly increased (even by 20 percent) and pump rangeability even improved with a better  $NPSH_i$  curve.

*Flow imbalance*—Field experience indicates that with double suction impellers the cavitation damage pattern (like pitting) may be different for each impeller eye, thus suggesting there is a flow imbalance between the inboard and the outboard eye of the impeller, which is forced by the upstream suction piping. This situation is clearly evident in Figure 42, which shows the bad effect of an elbow in the suction line even if followed by a straight pipe and a reducer.



*Figure 42. Cavitation Erosion with Double Suction Impeller and Bad Suction Piping (Bottom). Blade Suction Side: Heavy Sheet Cavitation Mode at  $NDE_{eye}$  (Top) and Absence of Damage at  $DE_{eye}$  (Middle). Vibrations Indicated the Presence of Suction Recirculation (No Blade Damage). ( $Q_{oper}/Q_{sl} = 0.70$ ,  $NPSH_A/NPSH_{3\%} = 1.5$ ,  $U_{eye} = 98$  ft/s, Cold Water, Impeller in 316SS,  $T_{service} = 2000$  Hours). Uneven Pattern of Sheet Cavitation and Suction Recirculation Is Related to Impeller Design, Operating Conditions, and Inlet Elbow.*

### *Scale Effects*

*Suppression pressure and fluid temperature*—With reference to damage mechanism it is thought that the erosion of the metal

surface exposed to cavitation is caused by a shock wave produced by the collapse (implosion) of each vapor bubble being a microsize (Tomita, et al., 1983). The induced impact pressure on the metal, which can reach a few kpsi, is strongly dependant from the pressure surrounding the vapor bubble (environmental pressure) before the collapse and also the surface tension of the liquid forming the bubble thin skin film, which is primarily related to the liquid temperature.

The effects of NPSH (suppression pressure) and temperature upon cavitation damage are shown in Figure 43, presents the results obtained for brass specimens by using the ASTM standard test method with vibratory apparatus (ASTM G32-85, 1985) and so the same cavitation intensity for all tests. The mean depth penetration rate (MDPR) is clearly increasing at any temperature with NPSH, which suggests that pumps operating with higher suction pressure and the same degree of cavitation (i.e., same cavitation number  $\sigma$ ) are subjected to higher damage rate. As an example it can be seen that at a temperature of 150°F for a change of NPSH from 35 ft to 140 ft (ratio 4) the MDPR increases from 0.055 to 0.425 inch/min (ratio 7.7). This situation could represent the case of a given pump operated at two speeds with ratio 2 ( $N_2 = 3580$  rpm,  $N_1 = 1790$  rpm) with similar cavitation condition, i.e., same  $\sigma$ , which imposes to increase the NPSHA with ratio  $2^2 = 4$ . However the damage rate increases with even higher ratio corresponding to  $2^3$  approximately. Recent research (Gülich and Pace, 1986) with actual pumps has demonstrated that in the cavitation regime of blade attached cavitation the erosion rate expressed as MDPR is proportional to NPSHA with exponent 3.

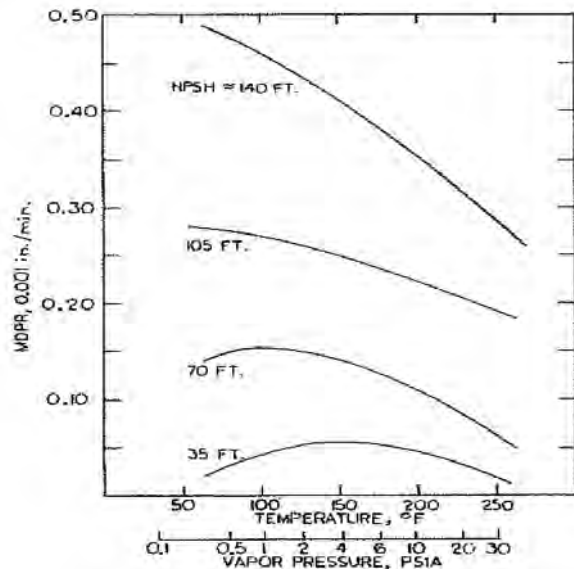


Figure 43. Effects upon Damage Rate (MDPR = Mean Depth Penetration Rate, 0.001 in./min) for Changes in Water Temperature and NPSH (Suppression Pressure) from Vibratory Tests with Bearing Brass Specimen. (Courtesy of Hammitt and Rogers, 1970; Cooper and Antunes, 1982)

The effect of fluid temperature on damage rate for 304 stainless steel specimens in water at constant pressure (one atmosphere) is shown in Figure 44. In this investigation, performed with the ASTM G32-85 procedure, the NPSH is actually decreasing with increasing temperature. The MDPR curve versus temperature shows a peak that might be related with material resistance variation (as linked to tensile strength) and NPSH change, thus reflecting the simultaneous influence of three factors, which in principle should be considered for establishing NPSHA margins.

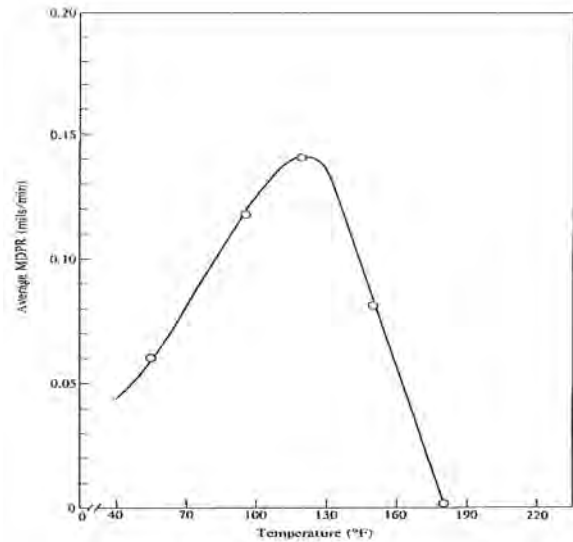


Figure 44. Effect of Temperature on Average Damage Rate (MDPR, mils/min) for 304 Stainless Steel Cavitated in Water at One Atmosphere Pressure. (Courtesy of Hammitt, 1980)

The thermodynamic effects reflecting the various fluid parameters involved in the cavitation process (inception and growth) and related with temperature are discussed above. The effects related with NPSHA (suppression pressure) fluid temperature represent scale effects.

**Pump speed and pump size**—Some effects of the pump speed are discussed above. Commonly the speed scale factor used is the parameter  $U_{eye}^2/2g$ , mainly reflects cavitation effects related with head. This scale speed parameter suggests cavitation variation with speed the same as expressed by affinity laws for capacity and head. However, this is seemingly true for dimensionless cavitation inception coefficient (for the same fluid and cavitation nuclei content), but it is not fully true for head degradation index (like 3 percent decay) and definitely not true for damage rate.

The effect of size, as geometrical scale factor has not been studied with clean approach by excluding the influence of other parameters (Deeproose and Herry, 1977).

#### Suction Specific Speed

By Hydraulic Institute definition, the NPSHR of a pump is the NPSH that will cause the total head (first stage head of a multistage pump) to be reduced by 3 percent (ANSI/HI 9.6.1, 1998). The suction specific speed is determined by using this value of NPSHR ( $S = N \times Q^{1/2}/NPSHR^{3/4}$ ) and so its value is associated with a fixed degree of cavitation in terms of head drop. The S parameter is “an index number for a centrifugal pump ... used to define its suction characteristic” (ANSI/HI 1.6, 2000). There are various recommendations and rules of thumb about safe S-values, like  $S = 8500$  US (generic opinion) and also critical values, like  $S = 11,000$  US (Hallam, 1982) or 10,000 US (limit specified by various companies). However the S-value for a given pump and impeller geometry numerically varies by looking at different capacities at constant speed. Although the HI standard does not explicitly indicate at which capacity the S-value should be referred, it is common practice in the industry to consider the BEP capacity for calculating the S-value. But the BEP capacity changes with:

- Impeller trim,
- Volute (vaned diffuser) design (e.g., simple change of throat).

In most cases the NPSHR curve is not affected by above geometrical and design changes as shown by tests. Then it frequently happens mainly among pump users and system designers to see technical

statements about pump reliability and acceptability based on  $S$ -values determined from pump curves (efficiency and NPSHR) for the specific job, which are significantly different from  $S$ -values derived for the same impeller with different outer diameter and different volute (vaned diffuser). By physical evidence and a large amount of experimental data, the most important capacity for characterizing the cavitation behavior is the shockless capacity, which is inherently determined by the impeller inlet geometry, i.e., invariable with the geometry of both the impeller exit and also volute (vaned diffuser) inlet. Therefore an  $S$ -value determined at the shockless capacity,  $Q_{sl}$ , would be truly more indicative of the pump suction characteristics and so constitute a more sound criterion for comparison with optimum values and critical limits. Certainly this  $S$ -criterion may present practical problems for wide industrial use. As an alternative option it should enforce the rule of determining always the  $S$ -value at the BEP capacity for the impeller design diameter, as the shockless capacity is not too far away (at least for more modern impeller designs).

The  $S$ -value is not unique for a given pump (i.e., inlet impeller geometry), but is influenced by many parameters, like the fluid temperature as discussed above. In Figure 45 the  $S$ -value is given for 5 percent head drop (more developed cavitation) and two capacity ratios ( $Q_o = \text{BEP capacity}$ ) versus the speed ratio at two different water temperatures. It appears that such  $S$ -value varies with temperature (not a definite trend), increases from high to low flow (as inferred from all NPSHR curves), and also increases nearly linearly with speed (not a general law) fully deviating from the affinity laws, which would imply invariance with speed ratio.

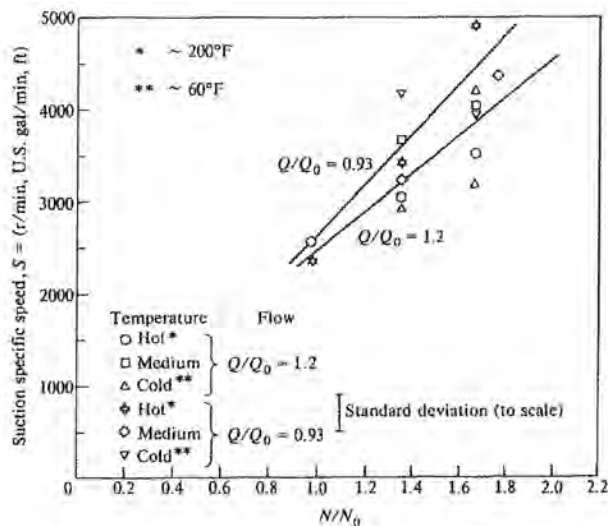


Figure 45. Suction Specific Speed Versus Normalized Pump Speed for Different Water Temperature and Two Capacity Ratios with 5 Percent Head Drop. (Courtesy of Hammitt, 1963, 1980)

Moreover the  $S$ -value is influenced by the flow pattern approaching the impeller and so the shape and size of the pump suction chamber, as the same impeller with an axial suction nozzle (overhung type, e.g., API - OH1) gives an  $S$ -value higher than with a side suction inlet (between-bearings, e.g., API - BB1). As a typical example:  $S = 11,000$  US for OH configuration and  $S = 9000$  US for BB configuration, which would lead to the erroneous conclusion using the above evaluation criteria that the OH pump is critical and (even not acceptable) and the BB pump with the same impeller is optimal (then acceptable). Actually the impeller with OH configuration operates better than with BB configuration particularly away from BEP capacity, thus having wider reliable operating range.

It is worth noticing that an  $S$ -value determined at the cavitation inception,  $S_{i-sj}$ , and the shockless flow,  $Q_{sl}$ , which can be

identified as  $S_{i-sj}$ , would have a more sound physical basis. The  $S_{i-sj}$  parameter would be a more meaningful index for comparing various designs and establishing optimal and likely critical ranges.

Historically the suction specific speed parameter was first introduced by Wislicenus, et al., in 1939. A close review of this basic reference along with a thorough discussion by several renamed pump designers (Wislicenus, et al., 1939), clearly shows more a conceptual approach with many assumptions than a truly scientific basis. In essence, the criterion for determining the reference cavitation degree is not quantitatively given, even if associated with head drop, while the extension of the experimental database used as backup is very limited with questionable physical relevance. In fact, the body of NPSH test data was obtained using the same impeller with several impeller trims, i.e., the basis covering the inlet impeller geometry was clearly not representative of the range of impeller inlet design parameters affecting cavitation behavior, even head decay.

#### Impeller Design and NPSHi-to-NPSHR Ratio

The majority of commercial pumps operate within the region defined by the NPSHi curve at top and the NPSHR curve at bottom, as the curve of NPSHA is between these two limits (single-stage type or first stage impeller with multistage type). The relative position of these two curves, namely the ratio NPSHi/NPSHR at given flowrate (as BEP percent) is a key factor for determining NPSHA margins, which are sound from both the technical and economic standpoints.

It is well-known that the impeller design, particularly the inlet geometry, is the primary factor determining the NPSHR value at design capacity (and so the  $S$ -value) along with the shape at off-design points. Also the level and shape of the NPSHi curve is by large given by the impeller design, as shown by visual cavitation inception investigations comparing different impeller geometries (Minami, et al., 1960; Bunjes, 1976; Schiavello, et al., 1988).

A thorough experimental investigation using both the acoustic method for cavitation inception (NPSHi) and the energy breakdown (at 3 percent) criterion, which covered a large number of commercial pumps (McNulty and Pearsall, 1979, 1982), provided interesting insights about the NPSHi/NPSHR ratio. Looking at Table 1, which presents a comparison of acoustic inception and 3 percent breakdown point for a more reduced number of pumps, it clearly appears that:

- The ratio NPSHi/NPSHR varies from 2.5 up to 16 depending on pump design and especially the operating point,  $Q/Q_{bep}$ . The lowest values are at 100 percent BEP (4.3 to 6.6) or even at 120 percent (2.5 or 3.6) suggesting a shockless flow close to such point. The highest values are always at part flows, even exceeding a 10 times factor.
- The  $S_b$ -value varies widely for each pump from inception,  $S_i$ , to breakdown,  $S_b$ . The pump with highest  $S_b$ -value (9243 US at BEP) shows the highest values for the ratio NPSHi/NPSHR in the operating range 50 to 100 percent, with the peak value at 75 percent (very likely close to suction recirculation onset). On the other hand pumps with lower  $S$ -values show lower ratios NPSHi/NPSHR.
- The volute pump ( $N_s = 2735$  US) in the last row shows the smaller values for the ratio NPSHi/NPSHR across a wide operating range (60 to 120 percent). The  $S_b$ -value at BEP is 6782 US, which would be considered as poor design by common opinion. However, the  $S_i$ -index has the highest values across the full table at same or close to  $Q/Q_{bep}$ , which means the lowest absolute NPSHi compared to all other pumps, including the cooling water pump with better  $S_b$ -value (9243 US). It is likely that this good cavitation behavior has been produced with an optimized impeller design. Essentially, this volute pump can operate with lower absolute NPSHA as compared to the cooling water pump, even having higher NPSHR ( $S_b = 6782$  versus  $S_b = 9243$  US).

The full trend of the ratio  $NPSHi/NPSHr$  in the capacity range from 50 to 120 percent BEP is presented in Figure 46 for four impellers with the same casing (first stage of boiler feed pump). Configuration 1 is the baseline impeller, which presented heavy cavitation damage, while Configuration 2, 3, and 4 are for three new design impellers, which were designed as alternative options for replacing the baseline impeller. Then all four impellers variants have the same design target (speed, flow, head) and would operate with the same NPSHA. The impeller eye diameter is smallest for Configuration 1, larger for Configuration 2 and 4 (same), and even larger for Configuration 3. Cavitation visualization investigations were performed with a transparent model of the full first stage (suction casing, impeller and discharge twin volutes casing) at full geometrical scale and half speed. Curves of  $NPSHi$  at visual cavitation inception (for bubble length of 0.08 inch = 2 mm) and  $NPSHR$  (3 percent drop) were determined for all four impellers. The visual cavitation was present on the blade suction (visible) side in the capacity range under study, which means up 120 percent BEP. Each curve has the lowest value at the maximum capacity around 120 percent. This is also the theoretical shockless flow for the three new design impellers (Configuration 2, 3, and 4), i.e.,  $Q_{sl}/Q_{ref} = 1.2$ , while the baseline impeller, Configuration 1, has much higher shockless flow. All the curves show a first peak value with decreasing flow at a capacity corresponding to stall incidence angle. It is worth noticing that the ratio  $NPSHi/NPSHr$  seems to increase with the peripheral eye velocity,  $U_{eye}$ , as shown by Configuration 3 with largest eye diameter, particularly in comparison with Configuration 2 and 4, which have a more consistent design approach. A detailed comparison is presented in Table 2, which also shows both the specific speed (nearly equal by design requirement) and also the S-value, which was changed by design choice. The ratio  $NPSHi/NPSHr$  is clearly increasing with the suction specific speed, S, and also the impeller eye velocity,  $U_{eye}$ . An impeller with low S and low  $U_{eye}$  (Configuration 1) seems to have a flatter curve  $NPSHi/NPSHr$ . However such an impeller would demand a high absolute value of  $NPSHi$  and so would demand a very high NPSHA to operate with zero/acceptable damage (and reasonable impeller life) as the  $NPSHr$  is too high. On the other hand an impeller with high S and high  $U_{eye}$  (Configuration 3) would still have a high absolute value of  $NPSHi$ , particularly at part flows, because of too high ratio, and would demand higher NPSHA/ $NPSHR$  ratio, because of high  $U_{eye}$ , leading to very high absolute NPSHA for acceptable cavitation. Then it appears that a medium S-value around 8000 US would be the best compromise to get zero/acceptable damage for the pump case presented with the given NPSHA.

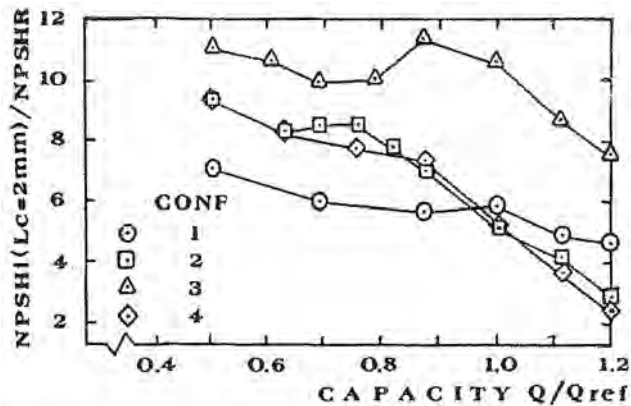


Figure 46. Ratio  $NPSHi/NPSHr$  Versus Capacity for Various Impeller Designs ( $i$  = Visual Inception with  $L_c = 2\text{ mm} = 0.08\text{ inch}$ ,  $r = 3$  Percent Drop). (Courtesy of Schiavello, et al., 1988a)

Table 2. Ratio Between Visual Incipient Cavitation and  $NPSHR_{3\text{percent}}$  (Cavitation Inception at  $L_c = 2\text{ mm} = 0.08\text{ inch}$ ). (Courtesy of Schiavello, et al., 1988a)

Impeller Configuration	1	2	3	4	
$Q_{bep} / Q_{ref}$	1.00	0.88	0.88	0.88	
Specific speed (at $Q_{bep}$ )	1605	1530	1425	1495	
$T_{bep} / T_{ref}$	1.000	1.020	1.035	1.050	
$H_{shutoff} / H_{bep}$	1.24	1.31	1.28	1.29	
Suction specific speed (at $Q_{bep}$ )	5800	8150	10100	8100	
$Q(NPSHi\text{-peak}) / Q_{ref}$	0.94	0.76	0.88	0.83	
$NPSHi\text{-minimum} / NPSHR$	4.7	2.9	7.5	2.4	
$NPSHi\text{-peak} / NPSHR$	5.9	(8.5)	11.3	7.4	
$NPSHi\text{-maximum} / NPSHR$	7.0	9.3	11.3	9.3	
$\left\{ \begin{array}{l} \frac{L_c}{L_{c,ref}} \\ \frac{L_c}{L_{c,ref}} \cdot NPSHA \end{array} \right\}$	Min flow (50%)	1.00	0.45	0.40	0.40
	$Q_{ref}$ (100%)	1.00	0.45	0.75	0.35
	Runout (120%)	1.00	0.35	0.50	0.20

The curves of the ratio  $NPSHA/NPSHR$  versus flow with given NPSHA are presented for the above case in Figure 47. The old design baseline impeller with lowest S-value and smallest  $U_{eye}$  (Configuration 1) shows the lowest NPSHA margin (high  $NPSHR$  along with low absolute NPSHA). This combined with inadequate design with high shockless flow and too steep inlet blade angle at hub caused heavy cavitation damage. The new design impeller with highest S-value and largest  $U_{eye}$  (Configuration 3) has clearly the highest NPSHA margin (smaller  $NPSHR$  with same absolute NPSHA). However cavitation visualization showed at the same NPSHA condition a much reduced cavitation but still too large a bubble, unable to ensure a reasonable impeller life (as will be shown later). On the other hand the impeller with intermediate S-value and also intermediate  $U_{eye}$  (Configuration 2 and 4) show NPSHA margins between the other two. The cavitation visualization at NPSHA showed for these two impellers very much reduced cavitation comparing to the two other impellers, which was acceptable for the expected impeller life. Then Configuration 2 impeller was chosen and exceeded the impeller life target of 40,000 hours.

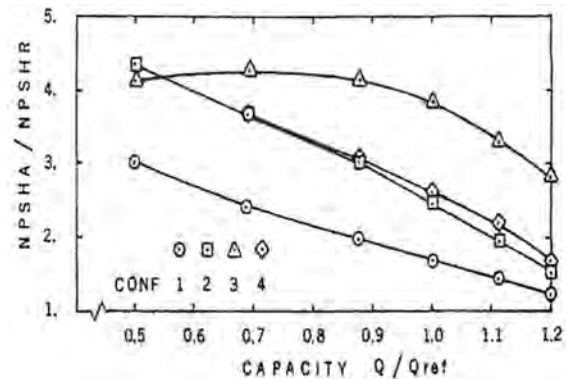


Figure 47. Classical Cavitation Margin Ratio  $NPSHA/NPSHr$  with Capacity for Different Impeller Variants with the Same Design Target of Flow-Head and Given NPSHA. (Courtesy of Schiavello, et al., 1988b)

All this leads to the main conclusion that the  $NPSHA/NPSHR$  margin has to be closely linked with both the impeller design and also the peripheral eye velocity, which likely leads to exclude low or high S-values also depending on the absolute NPSHA.

*NPSHA Margins—Main Clues*

*Literature information*—There is strong demand in the pump industry for sound criteria and simple guidelines establishing NPSHA margins, expressed as:

- The difference  $NPSHA-NPSHR$ ,
- And/or the ratio  $NPSHA/NPSHR$ ,

which would be applicable to different pump services. Basically these margins are needed by:

- The system designer for ensuring adequate NPSHA,
- The pump manufacturer for making appropriate pump selection (design, size, and speed), and
- The pump user for achieving expected reliability.

A search of the published literature showed various and widely heterogeneous recommendations reflecting different technical background and personal experience. Some simple guiding rules provided by pump designers (Florjancic, 1982; Cooper and Antunes, 1982) are useful, even if empirical. Considering society standards, guidelines were published by the Hydraulic Institute (ANSI/HI 9.6.1, 1998), which were based on the parameter called suction energy and linked to the S-value,  $U_{eye}$ , plus other factors for three suction energy levels. However these guidelines were drafted and presently are being revised. The draft of API-610, Eleventh Edition, which was still under revision in 2007, includes statements concerning high energy pumps and NPSHA requirements for target impeller life. Moreover, several internal guidelines can be found with:

- Pump manufacturers (even different rules within the same company),
- Engineering companies' specifications,
- End users' requirements (varying with industry and pump service: oil, chemical, fossil power, nuclear power, etc.).

All this information actually gives the impression of moving in a jungle, reflecting both the complexity of the issue and the inadequacy of present data/approaches.

*Key factors*—With specific focus on cavitation damage the relative importance (rank) of the various parameters can be inferred by considering the cavitation physics, experimental laboratory data, shop test data and also a wide range of field observations. Then relative rank (Schiavello, 1993) can be assessed by assuming a reference level of influence (taken equal to 1) and assigning a relative severity level to each factor. In the list below the key factors are given with a rank range (in bracket) putting the parameter with paramount importance at the top.

- Peripheral velocity at impeller eye ( $U_{eye}$ ) (8 to 10)
- Pump design, primarily the impeller ( $Q_{sl}/Q_{bep-des}$ ,  $Q_{rs}/Q_{bep-des}$ , special design features) and secondarily the suction chamber (5 to 7)
- Operating capacity ratio (as fraction of  $Q_{sl}$ , preferably, or  $Q_{bep}$  at maximum impeller diameter for less critical duties) (4 to 7)
- Ratio NPSHi/NPSHr (4 to 6)
- Liquid density (SG) (4 to 5)
- Impeller material resistance to cavitation erosion:
  - Commercially available alloys (2 to 4),
  - Special patented alloys excluding (5 to 7)
- Corrosion (various types: chemical, galvanic, etc.) (2 to 4)
- Fluid temperature (worse if low) (1 to 4)
- Air content (noncondensable gas content, more generally) (1 to 4)
- Vapor density (1 to 3)
- Thermodynamic fluid properties (specific heat, vaporization latent heat) (1 to 3)
- Suction specific speed (1)

Clearly the above parameters should be included in any quantitative model for NPSHA margins (like a ratio NPSHA/NPSHR) along with the quantification of their respective role even with a

statistical relevance. Presently this kind of quantitative correlation is yet undefined even for restricted homogeneous range of pump applications (e.g., water services).

## IMPELLER LIFE EXPECTANCY

### *Modern Approach*

From the above data and considerations it is evident that for the majority of industrial pump designs, which must comply with several and conflicting requirements (efficiency, wide range reliability, overall dimensions and speed, cost, etc.), the cavitation inception curve, NPSHi, can be much higher than the conventional 3 percent drop curve, NPSHR. In principle a requirement for total absence of cavitation and so zero damage (unlimited impeller life) would dictate NPSHA close or above NPSHi across the whole operating range. However in practice this requirement leads to an anti-economic design of both the system and the pump.

In special cases (nuclear power plants) some end users impose in their specifications for the reactor feed pump (high speed and high energy) the requirement of zero visual cavitation within the preferred operating range (POR), which must be fully proven making flow visualizations with model pump tests (model size and speed to be agreed). In this case there is always a booster pump at lower speed, for which less stringent cavitation requirements are given allowing a certain amount of internal cavitation. The total head specified for the pumping unit can be shared between the booster pump and the main feedwater pump, which helps to accommodate the requirement of zero cavitation for the main pump by a proper selection of the booster head and main pump speed. However the overall efficiency (booster and main) is penalized plus the entire cost, including cavitation visualization model tests, is very high, which appears justified only for a very selected category of pump applications. In this case the specification requirement is NPSHA > NPSHi and the curve of NPSHi within the POR, must be determined with model tests (even CFD predictions are not accepted).

In the majority of industrial pump applications so far (covering several decades) the curve of NPSHA is certainly below NPSHi and above NPSHR, which means that cavitation is surely present with effects, which can be tolerated (millions of field pumps with satisfactory and long services) or may cause problems (hundreds or thousands of field pump troubles clearly diagnosed with cavitation as the root cause). Starting from the 70s the number of field cavitation problems, primarily heavy and quick impeller damage, and the inherent overall cost (including loss of production) have drastically risen particularly for critical pumps, operating with either high speed (feedwater, water injection) or wide range (water circulation), which induced extensive cavitation visualization investigation. The reasons of field cavitation damage were understood and solutions found (like new impeller design) also by accepting a certain amount of cavitation damage suitable to ensure a reasonable period of service time with trouble-free operation. Also it was evident that an economic choice of the NPSHA optimizing the overall cost (installation and operation) of the system and the pump should allow the occurrence of cavitation damage under controlled conditions. This led to a new approach for NPSH requirement based on acceptable damage ( $NPSH_d$ ,  $d$  = damage) and impeller life (impeller life expectancy).

This new approach has been used in the last 20 years in specific cases and by individual companies with different requirements. In general a modern approach for cavitation requirements using the life expectancy target should:

- Establish the life criterion (typically: metal damage).
- Identify the pump components susceptible of cavitation damage (usually: impeller).
- Define the damage parameter (mean depth penetration = MDP, weight loss = WL, damaged area = DA, other index).

- Establish the damage entity allowance.
- Give the value or criterion for the life time (cumulative service, hours or years).
- Associate a confidence level (like expectancy probability).

Presently there are basically two methods, which were introduced in the 80s and are used for specific projects by direct demand of the end user. Although the ultimate objective is the same (impeller lifetime in presence of cavitation), the actual output provided by the pump designer to the end user is different, i.e.:

- NPSH required for given impeller life of 40,000 hours (NPSH<sub>40,000</sub>). With this method the curve of NPSH<sub>40,000</sub> versus capacity over a specified operating range is provided. The method developed by Vlaming (1981, 1989) and described above follows this approach. Also some additional data are requested (Qsl, Qrated/Qsl, operating range, D<sub>eye</sub>, inlet blade angle, U<sub>eye</sub>) for the verification of end user. However, this method has strong limitations because:

- It is empirical,
- Damage allowance is not formulated,
- It is valid only for cold water and stainless steel impellers.

- Impeller life expectancy with associated probability. With this method the pump designer is requested to ensure a given impeller life, which is usually specified by the end user along other parameters including NPSHA and operating mode (see below). This method (Gulich and Pace, 1986; Gulich, 1989a) is based on the prediction of cavitation erosion using the correlation based on:

- Cavity length (L<sub>cav</sub>), or
- Cavitation noise level (CNL).

The approach with cavity length, L<sub>cav</sub>, is presented below along with applications.

#### *Impeller Life Expectancy Assessment*

##### *Cavitation Erosion Prediction with Cavity Length, L<sub>cav</sub>*

Gulich's correlation for predicting the cavitation erosion rate based on cavity length, L<sub>cav</sub>, is discussed briefly above and shown in Equation (9) after restructuring with Equation (10) using dimensionless parameters (τ<sub>A</sub>, φ) and also limiting water at two fluid temperatures. The correlation is given in Equation (42) with full original formulation (Gulich and Pace, 1986; Gulich and Rösch, 1988; Gulich, 1989a, 1989b) for the scope of the subsequent discussion, including independent validation and follow up applications.

$$E_R = C_L \left( \frac{L_{cav}}{L_{cav,R}} \right)^{\lambda_2} \frac{(P_0 - P_{sat})^3 F_{cor}}{R_m^2 F_{Mat}} \left( \frac{\alpha_R}{\alpha} \right)^{0.36} \left( \frac{a}{a_R} \right) \left( \frac{\rho_R}{\rho} \right)^{0.44} \quad (42)$$

with:

$$C_L = \begin{cases} 7.92 \cdot 10^{-6} \text{ mm h}^{-1} \text{ Pa}^{-1} \text{ for blade suction side (C}_{SS}) \\ 3.96 \cdot 10^{-4} \text{ mm h}^{-1} \text{ Pa}^{-1} \text{ for blade pressure side (C}_{PS}) \end{cases}$$

$$\lambda_2 = \begin{cases} 2.83 \text{ for suction side} \\ 2.6 \text{ for pressure side} \end{cases}$$

$$\begin{aligned} L_{cav,R} &= 10 \text{ mm} \\ a_R &= 1490 \text{ m/s} \\ \alpha_R &= 24 \text{ ppm} \\ \rho_R &= 0.0173 \text{ kg/m}^3 \end{aligned}$$

In Equation (42) the parameter definition is: E<sub>R</sub> = erosion rate (mm/h), L<sub>cav</sub> = cavity length (mm), P<sub>0</sub> = static pressure at impeller

inlet (N/m<sup>2</sup>), P<sub>sat</sub> = saturation pressure (N/m<sup>2</sup>), F<sub>cor</sub> = corrosion factor, F<sub>Mat</sub> = material factor, R<sub>m</sub> = tensile strength of impeller material (N/m<sup>2</sup>), α = gas content of liquid (ppm), a = speed of sound of liquid (m/s), ρ' = density of saturated vapor (kg/m<sup>3</sup>). The subscript for some parameters on the right side of Equation (42) stands for reference values, which are given above.

The quantitative definition of the erosion rate is given by Equation (43):

$$E_R = \text{MDP} / T \quad (43)$$

where MDP is mean depth penetration (mm) and T is time (h).

The above correlation (43) is supported (Gulich and Pace, 1986; Gulich, 1989a) with tables with:

- The values for F<sub>cor</sub> and F<sub>mat</sub>,
- The range of parameters used for its generation, which basically constitutes the range of application,
- The scaling effects as inferred from the formula.

It is worth noticing that according to Equations (9), (10), and (42) the erosion rate varies with: U<sub>eye</sub><sup>6</sup>, NPSH<sup>3</sup>, ρ<sup>3</sup>, R<sub>m</sub><sup>-2</sup>, L<sub>cav</sub><sup>2.7</sup> (average exponent between suction side and pressure side, but C<sub>PS</sub> = 50 C<sub>SS</sub>), and fluid temperature (secondary and more complex effect). The coefficients C<sub>PS</sub>, C<sub>SS</sub> are strictly related with the impeller design, while the parameter L<sub>cav</sub> depends on both the impeller design and the NPSHA level in relation to NPSHi (i.e., the ratio NPSHA/NPSHi rather than the ratio NPSHA/NPSHR). Equation (42) clearly shows that the cavitation damage is linked to pressure level at impeller suction and not to impeller head. All these remarks should be in mind for establishing NPSHA margins.

The E<sub>R</sub> correlation was derived from a database widely scattered (Gulich and Pace, 1986) and suggested a statistical analysis of the frequency distribution of the data points. This permitted to quantify and associate a probability index to the impeller life predictable with the correlation. The curve in Figure 48 links the probability P (percent) of reaching an impeller life specified to the ratio R between required and calculated impeller life given in Equation (44):

$$R = I_{L,Req} / I_{L,cal} \quad (44)$$

where I<sub>L,Req</sub> is the desired impeller life (target) and I<sub>L,cal</sub> is the impeller life calculated using the correlation and the following equations:

$$\text{MDP}_{\text{tot-cal}} = \Sigma \tau_{\text{oper}} E_R \quad (45)$$

$$I_{L,cal} = \text{MDP}_{\text{all}} / \text{MDP}_{\text{tot-cal}} \quad (46)$$

where MDP<sub>all</sub> is mean depth penetration allowed, MDP<sub>tot-cal</sub> is the total or cumulative damage, E<sub>R</sub> is the erosion rate for each flowrate or operating point, τ<sub>oper</sub> is the fraction of the time that the impeller is expected to operate at that operating duty (flow and other associated conditions), and MDP<sub>all</sub> is mean depth penetration allowed. Figure 48 shows that a probability around 90 percent corresponds to R value of 0.5, which means that the predicted impeller life should be at least twice the target (as example: I<sub>L,Req</sub> = 40,000 hours, I<sub>L,cal</sub> = 80,000 hours). With reference to MDP<sub>all</sub> it basically represent the impeller life term as indicated in the specifications (e.g., in several cases a value corresponding to 0.75 of the blade thickness at the location damage has been mutually agreed between pump designer and end user).

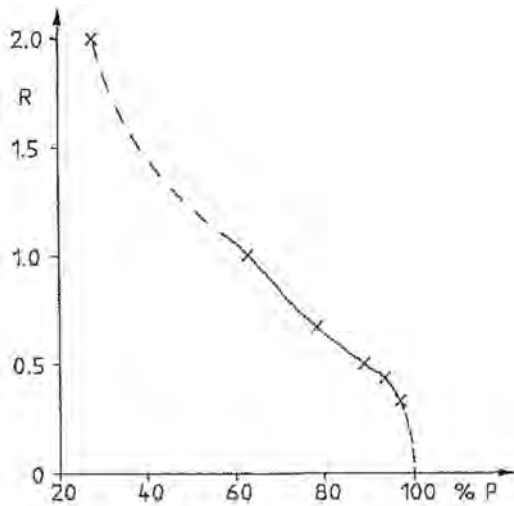


Figure 48. Probability Function for Impeller Life Prediction from Cavity Length. (Courtesy of Gülich and Rosch, 1988; Gülich, 1989a)

#### Independent Validation with Field Data

A field cavitation problem that occurred in the mid 80s was chosen for verifying the validity of the above cavitation damage prediction method basically using data that surely were not included in the backup database of the correlation. The field problem concerned four full capacity main boiler feed pumps operating in the same power plant. Each pump was turbine driven with its booster and could be operated at variable speed. The plant, having four generating units (Unit 1 through 4) of 660 MW each, had been originally planned for base and high loads. The pump design target was:  $N = 5200$  rpm,  $Q = 10,400$  gpm,  $H = 12,580$  ft,  $NPSHR = 325$  ft,  $NPSHA = 560$  ft (= 1.7 times  $NPSHR$ ). The pump had six stages with a power per stage around 6300 hp, indicating a very high energy pump.

The four units had different operating histories. In March 1986 the feedwater pump of Unit 1 with the longest service time was stopped because of a bearing vibration problem, which was later identified as a structural resonance of the bearing housing at vane pass frequency. An internal inspection of the pump rotor revealed the presence of severe cavitation damage in the first stage impeller. Thereafter, the inspection was extended to the other feedwater pumps (Unit 2, 3, and 4) revealing similar damage characteristics for all four pumps with different extension and depth. Basically, the cavitation damage was concentrated (Schiavello, et al., 1988) primarily at the corner between the suction side of the blade root and the impeller hub with some extension on the blade visible side at the hub section. Actually the cavitation erosion perforated all the way through the impeller hub thickness and also penetrated into the shaft. There was no damage at all on the blade pressure side. With today's knowledge the damage pattern would be associated with the mode of corner cavitation (primary mode) and also blade attached cavitation on the hub section (secondary mode). Record data of the actual operating mode were obtained from the plant control room, including: plant load (MW), feedwater pump speed (rpm), and head (ft),  $NPSHA$  (ft), and actual operating time at each load. The analysis of these field data permitted to derive the pump flow at each load and also reconstruct the time operating mode, giving both the total service time and fraction operating time at each plant load and pump flow ( $\tau_{oper}$ ). The total operating time was 14,000 hours for Unit 1, which presented a cycling load operating mode (more than 50 percent of time at part load) with pump running at part flows below BEP. Unit 4 had a total operating time of 6000 hours characterized with a basic load operating mode (about 70 percent of time) and consequently a feedwater pump running near the design conditions.

With varying plant load the pump speed was also varied decreasing from high plant loads (500 to 600 MW) down to low loads (300 MW) and correspondingly the actual impeller eye velocity was ranging from 200 ft/s to 170 ft/s.

A new design impeller was considered as the most effective first step to reduce the cavitation damage. A first impeller design option was urgently developed and installed in the plant in October 1986 also upgrading the material from CA15 to CA6NM. However, a parallel extensive program of cavitation visualization tests with a model pump (full geometrical scale and half speed) on several impeller variants was planned to cover alternative design options with the aim to identify the best solution for late field implementation, if necessary. This experimental investigation was carried out in early 1987. Four impellers were tested, including the original design with heavy damage (baseline A) plus three variants with new design (B, B1, and BM) also identified as Configuration 1, 2, 3, and 4, respectively (Table 2, Figures 46 and 47).

The field cavitation conditions were simulated for the cavitation visualization with the model test by reproducing similar  $NPSHA$  according to affinity laws ( $\tau_{Am} = \tau_{Af}$ ,  $m =$  model test,  $f =$  field pump). Then the corresponding cavitation bubble length  $L_{c,b}$  ( $b =$  visual vapor bubble) was determined in the full operating range,  $Q/Q_{ref} = 0.5$  to 1.2 (ref = BEP capacity of impeller A). The curves of  $L_{c,b}$  normalized with the same reference  $L_{c,b,ref}$  (bubble length at BEP of impeller A) are presented in Figure 49 for all four impellers. For impeller B (Configuration 2) the bubble length  $L_{c,b}$  was drastically reduced across the entire operating range. Further reduction of  $L_{c,b}$  was obtained with impeller BM (Configuration 4) by grinding the vane suction surface at inlet. The cavitation bubble length was also reduced with impeller B1 (Configuration 3) but less than for impeller B and BM (Configuration 2 and 4). It is worth noticing that although the new design impeller B1 (Configuration 3) has higher S-value and so higher margin ratio  $NPSHA/NPSHR$ , it presents more extended cavitation (higher  $L_{c,b}$ ) over the full capacity. This is due to higher impeller eye velocity (ratio 1.05).

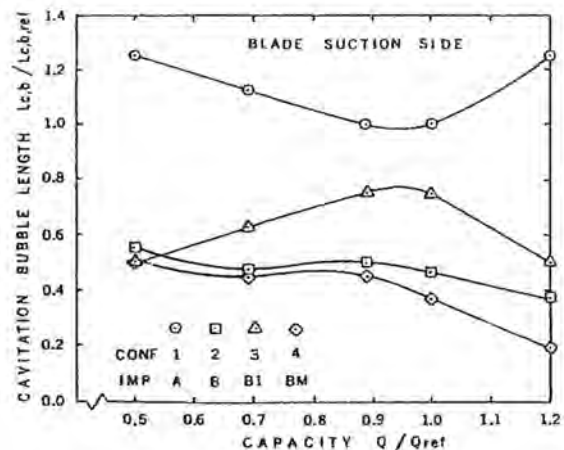


Figure 49. Cavitation Bubble Length at Plant  $NPSHA$ . (Courtesy of Schiavello and Prescott, 1991)

Then Equation (42) was applied to calculate the cavitation erosion rate  $E_R$  by using:

- The visual cavity length ( $L_{cav} = L_{c,b}$ ) with a justified assumption of no scale effect for speed, and
- Actual field conditions for all other parameters.

The curves of  $E_R$  over the full capacity range are shown for all four impellers in Figure 50. It appears that the cavitation erosion rate  $E_R$  is reduced by at least a factor 10 for the impeller B and BM as

compared to the baseline impeller A, while the reduction is much less pronounced for the impeller B1 (with higher S-value and larger NPSHA/NPSHR, but higher  $U_{eye}$ ).

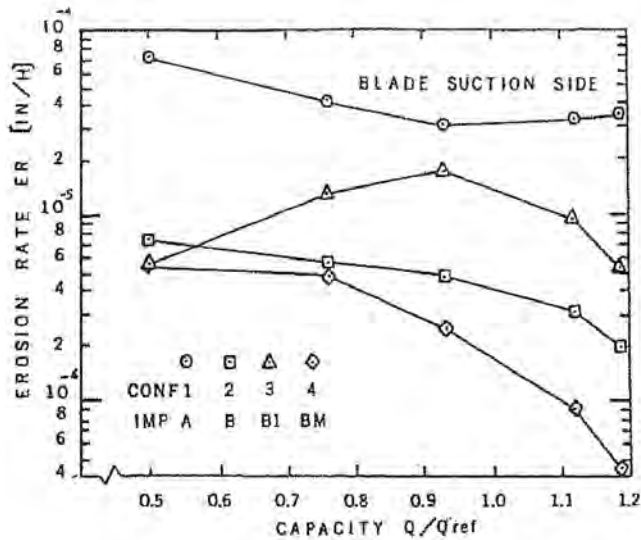


Figure 50. Erosion Rate on Blade Suction Side Versus Capacity. (Courtesy of Schiavello and Prescott, 1991)

Equation (45) was used to determine the  $MDP_{tot-cal}$  for the baseline impeller A with actual field data of fraction operating time ( $\tau_{oper}$ ) for both the generating Unit 1 and Unit 4. Also, the same procedure based on  $L_{c,b}$  from visualization model data (Figures 49 and 50) was applied with the new design impeller B installed in Unit 1, which was routinely inspected and presented some damage (suitable to achieve the target life of 40,000 hours). A comparison (Schiavello and Prescott, 1991) with actual damage depth ( $MDP_{act}$ ) showed for all three cases (impeller A with Unit 1 and Unit 4, impeller B with Unit 1) that by using the visual bubble length (from model tests),  $L_{c,b}$ , the theory underestimates by 40 percent the erosion depth. Then Equations (42) and (45) were applied by using as input a damage cavity length ( $L_{cav} = L_{c,ed}$ , ed = erosion depth), which was measured at the point of maximum depth in the damaged impellers (A-Unit 1, A-Unit 4) or obtained with damage model tests using a soft paint technique (impeller B-new operating mode of Unit 1). The comparison with  $MDP_{act}$  was very satisfactory for all three cases.

The analysis of three field cases was extended to obtain the similarity parameter for cavitation erosion,  $\theta_L$ , used by Güllich and Pace (1986), which is related to the erosion rate as follows:

$$\theta_L = K_\theta E_R \quad (47)$$

The values of  $K_\theta$ , which includes all parameters all factors linked in Equation (42) with operating conditions and fluid properties plus impeller material, were derived from actual field data. The value of  $E_R$  was derived using damage cavity length ( $L_{cav} = L_{c,ed}$ ). The actual field values of  $\theta_L$  are plotted in correspondence of  $L_{c,ed}$  in Figure 51, which is reproduced from the original Güllich paper with publication of the cavitation erosion prediction methods. It is evident from Figure 51 that both the old design impeller A (Unit 1 and Unit 4) and the new design impeller B (Unit 1) fall within the correlation database. It is worth noticing that the new design impeller B with Unit 1 clearly shows a low cavitation erosion index ( $\theta_L$ ) and a small damage cavity length ( $L_{c,ed}$ ), which are close to the best cases (only a few) covered by the database. In fact this impeller is more recent field data have confirmed that this impeller has exceeded the life target of 40,000 hours.

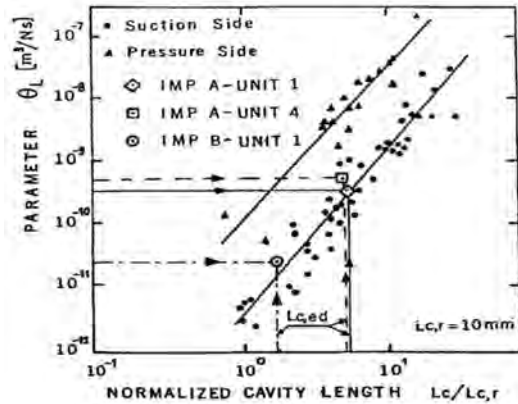


Figure 51. Field Cases (Impeller A and Impeller B) Compared with the Database of the Cavitation Erosion Prediction Correlation Compared. (Courtesy of Schiavello and Prescott, 1991; Güllich, 1986)

Basically from the above discussion it can be inferred that the validity of the prediction method given by Equations (42) and (45) is acceptable and is enhanced if sound input values are available for  $L_{cav}$ . In general, it seems that the cavitation erosion is somewhat underestimated predicting an optimistic impeller life,  $I_{L,cal}$ , if the visual cavitation bubble from model tests,  $L_{c,b}$ , is simply used without applying a correction factor (higher than 1). This might be derived from model test with soft paint. Alternatively the theoretical  $MDP_{tot-cal}$  could be increased by 50 percent (as inferred from the field comparison discussed above) or even more. Moreover the broad scatter of the correlation database (Figure 51) and the large uncertainty about actual field operating conditions (like the parameter  $\tau_{oper}$ ) clearly suggests to always enforce a high probability value along with the impeller life target. This probability also depends on the soundness of the input parameters in Equation (42), particularly the cavity length,  $L_{cav}$ .

The three field cases discussed above for assessing the validity of the cavitation erosion correlation based on  $L_{cav}$  given by Equation (42) cover cavitation damage on blade suction side with the cavitation modes of both the blade attached cavitation and corner cavitation. The correlation covers also the damage on the blade pressure side, which can be produced either at high flows (cavitation mode of blade attached cavitation) or at low flows (cavitation mode of vortex cavitation driven by suction recirculation) as discussed above and shown in Figure 40. Then it is not clear if the correlation is applicable for both such cavitation modes or to one only.

Actual data of field cavitation damage concerning a high energy boiler feed pump operating in five power plants (600 MW) at part loads and so low flows ( $Q/Q_{bep} = 0.43$  to  $0.63$ ) were published by Van Der Westhuizen (1992). The location of damage was found for all five pumps on the blade pressure side with appearance that is typical of vortex cavitation caused by suction recirculation. This is easily deduced by looking at the operating flowrates (the highest at 63 percent  $Q_{bep}$ ) and confirmed in the paper. The similarity parameter  $\theta_L$  given by Equation (47) was obtained with actual field value of  $E_R$  (as  $MDP_{actual}/T_{tot-oper}$ ) and compared with the correlation database (in the same way done in Figure 51). The five field values of  $\theta_L$  are plotted in correspondence of the respective actual  $L_{c,dam}$  (dam = damage) and fall significantly away from the fit line for pressure side cavitation erosion, which is represented by Equation (42) with values of  $C_L$  and  $X_2$  for pressure side.

From this comparison it can be deduced that the cavitation erosion correlation based on  $L_{cav}$  and given by Equation (42) is not applicable for predicting cavitation damage caused by the vortex cavitation in presence of suction recirculation, i.e., for pumps operating at low flows ( $Q_{oper} < Q_{rs}$ ).

Then it seems that the application of Equation (42) for predicting pressure side cavitation is restricted to operations at high flows ( $Q_{oper} > Q_{sl}$ ) in the regime of blade attached cavitation.

*Impeller Life Expectancy*

*Calculation—Practical Example*

The above approach for assessing the impeller life expectancy was applied with a case of power plant rerate for pump upgrade evaluation as demanded by the end user. The case (Schiavello and Prescott, 1991) was regarding a single main boiler feed pump (100 percent capacity) of a 330 MW power plant. The pump, which was motor driven, operated with variable speed. The pump, which had eight stages and a double suction impeller in the first stage, was directly fed by a deaerator located at higher elevation. The pump was designed in 1965 for base and high load duties with original conditions of service (COS) specified as:  $N = 3420$  rpm,  $Q = 6100$  gpm,  $TDH = 9140$  ft,  $NPSHR = 51$  ft. The first stage impeller was designed with  $S = 9900$  US per eye with a peripheral velocity at the impeller eye of 145 ft/s and so can be considered as relatively high energy/high speed stage.

A field survey in August 1988 showed that the first stage impeller had suffered some metal damage. The damage area was located on the pressure (hidden) side of each blade, but only on the inboard impeller eye (pump coupling side). No damage was noticed on the impeller eye at the outboard side. A panel of experts concluded that the damage was caused by the suction recirculation due to both operation at part load and a flow imbalance between the two impeller eyes. They recommended redesigning the first stage impeller to lower the suction recirculation and also reduce the sensitivity to uneven repartition of the capacity. Moreover the plant operator intended to change the operating mode of the plant from basic load to cycling load down to 100 MW requesting a new reliable minimum flow. Then the end user made a specific request of a new design first stage impeller with the suction recirculation onset capacity shifted below the new minimum plant load (100 MW) and also asked to provide the impeller life assessment.

Then the pump designer established a solution methodology described below:

- Step 1—Operator input (plant data). The plant operator was requested (August 1989) to supply data of the expected pump operating profile, as key input to the impeller design target. Such data included the base operating mode plus two potential alternatives. Also the impeller life target was agreed for 40,000 hours ( $I_{L,req}$ ) associated with an acceptable maximum erosion depth,  $ED_{max}$ , equal to 75 percent of blade thickness ( $ED_{max} = MDP_{all} = 0.75 T_b$ ,  $T_b$  = blade thickness). Moreover, the plant operator was convinced to revise the original COS and possibly limit the highest flow capacity (at plant full load) to the really expected service, in order to optimize the design of the impeller for part flow operations. The pump operating line is shown in Figure 52 along with the pump performance map.

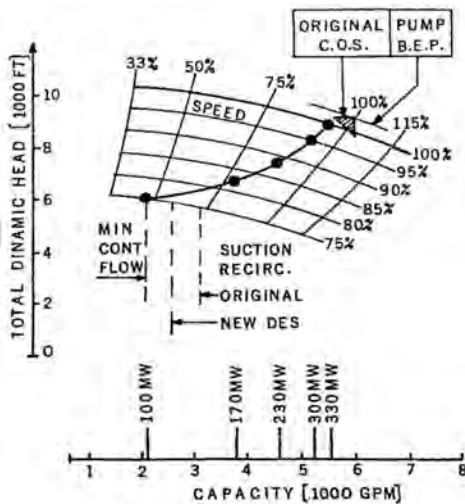


Figure 52. Pump Performance Map and Operating Line. (Courtesy of Schiavello and Prescott, 1991)

- Step 2—Impeller design strategy. An impeller design was developed aimed at achieving the specified life of 40,000 hours with high probability. The full range of the operational parameters (capacity, speed, NPSHA) was analyzed as shown in Figure 53. The erosion rate prediction curve was derived for a preliminary impeller geometry by applying Gülich's correlation with cavity length given by Equation (42). The variation of  $L_{cav}$  with capacity and NPSHA geometry was inferred from an internal database of cavitation visualization model tests.

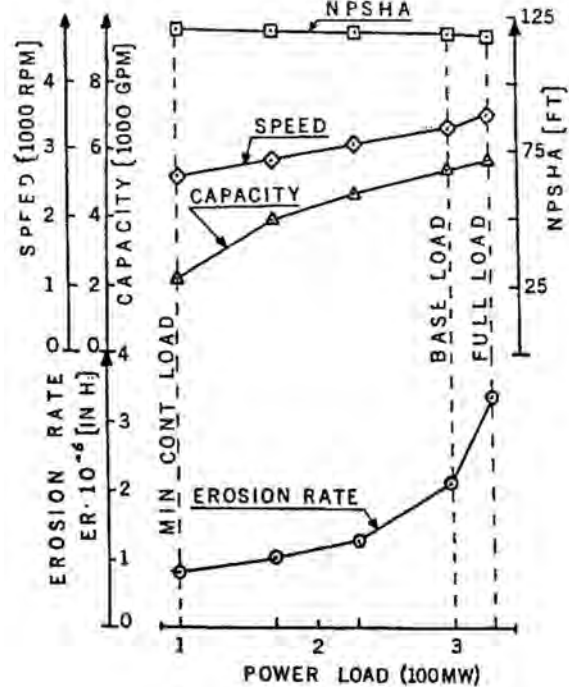


Figure 53. Operating Parameters and Cavitation Erosion Rate. (Courtesy of Schiavello and Prescott, 1991)

It is clear from Figure 53 that the tendency to cavitation erosion is higher at the base load (300 MW) and, especially, the full load (330 MW), while it is lower at part load. This shape of the ER-curve rapidly decreasing with plant load seems to be peculiar of a pumping configuration with variable speed main feedwater pump and deaerator (i.e., essentially constant suction pressure) which leads to the amplification of the NPSHA margin as the load is reduced. It is also important to note that the erosion rate has a tendency to sharply rise at high flow/high speed. This aspect suggests that an overflow at the inboard impeller eye, which is being forced by a flow imbalance between the inboard and outboard eye of the impeller and is producing a negative incidence angle, is the most likely cause of cavitation damage over the blade pressure side (blade attached cavitation) in this installation, rather than a suction recirculation related damage (vortex cavitation).

The predicted cumulative damage erosion depth (ED) expressed as percent of blade thickness was compared for the three cases of the pump operating profiles, i.e., base load, Alternative 1 (full load at 300 MW) and Alternative 2 (unit operating in partial load condition) as shown in Figure 54. It is evident that Alternative 1 is the most severe in terms of cavitation damage. Then the new impeller geometry was finalized by selecting the shockless capacity for the full load operation at 330 MW. The cumulative damage prediction was also made for an impeller life of 60,000 hours with the aim of producing a more complete assessment of the impeller life expectancy and is also shown in Figure 54. It is evident that the expected overall damage should not reach 75 percent of the blade thickness, even after 60,000 hours and Alternative 1.

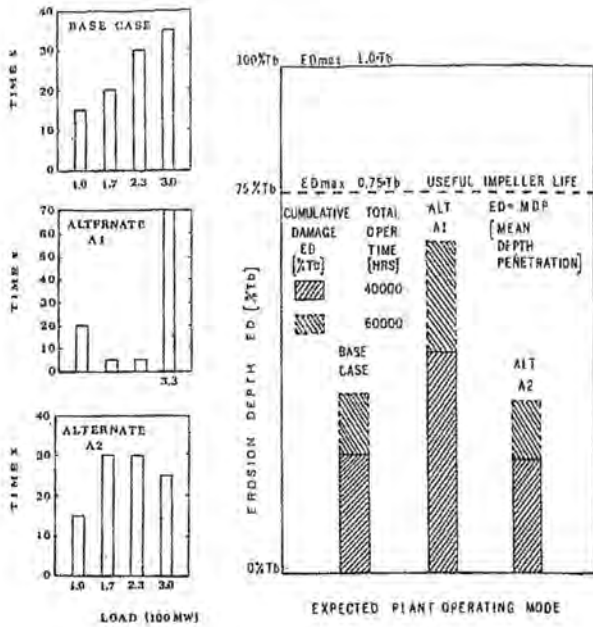


Figure 54. Cavitation Cumulative Damage as Predicted with Three Plant Operating Modes. (Courtesy of Schiavello and Prescott, 1991)

The probability (Gulich and Rosch, 1988) of achieving an impeller life of 40,000 hours (operator realistic target) and even 60,000 hours (operator ultimate goal) was also analyzed as shown in Figure 55. In general, the situation is quite satisfactory with a lower probability of 68 percent for Alternative 1/60,000 hours.

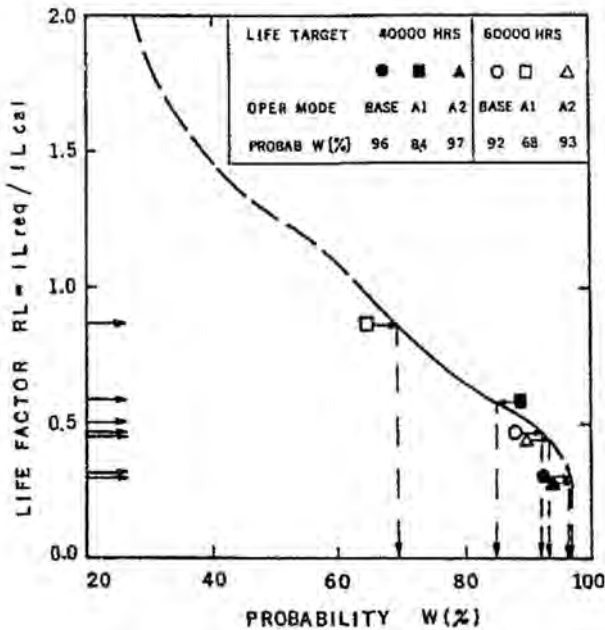


Figure 55. Assessment of Impeller Life Expectancy. (Courtesy of Schiavello and Prescott, 1991)

• Step 3—Suction casing modifications. A close review of the side suction casing suggested that the flow imbalance between the inboard eye and outboard eye of the impeller was likely caused by an internal asymmetry producing different hydraulic resistance for the inboard and outboard flow path. Then appropriate geometrical changes were made in the suction casing aimed at producing equal flow sharing, which was the basis of the new impeller design and life assessment presented above.

The boiler feed pump with the above modifications was started in July 1990. Some feedback information one year later from the plant operator indicated that the pump operated reliably from 100 MW to a full load of 330 MW, as desired. No concerns have been expressed by the plant operator since 1991.

In essence Figures 53 and 54 present a complete picture of the assessment of impeller life expectancy, including various options for the end user in relation to:

- Potential plant operating mode,
- Desired impeller life target,
- Acceptable impeller damage, and
- Associated probability.

#### Impeller Life Expectancy Enhancement

##### Advanced Impeller Design

New criteria for impeller hydraulic design have been developed from the mid 70s to the present with the aim of reducing the cavitation erosion rate in a wide operating range and enhance impeller life expectancy. Basically the new design strategies were finalized for the following objectives:

- Minimize cavitation erosion mainly at part flows, i.e., flatten the NPSHi curve for sheet cavitation-suction side and possibly eliminate the corner cavitation. First, the selection of the shockless capacity was carefully considered in relation to the expected operating range and the plant operating mode, requesting input from the plant operator. Second, the entire geometry of the blades from the hub to the tip at the impeller inlet (angle, thickness, and vane shape) was optimized to reduce the cavitation bubble length. The design objective was to avoid high peak of local velocity close to the blade leading edge at off-design, as initially suggested from basic fluid dynamics plus experimental investigation with cavitation visualization, and more recently shown by theoretical simulation with full CFD studies.
- Lower the onset of suction recirculation capacity and reduce or even eliminate the risk of to vortex cavitation within the operating range. This was made possible by the application of advanced design criteria for minimizing suction recirculation (Schiavello and Sen, 1980, 1981).

The effectiveness of these new design criteria for the impeller has been fully proven in the laboratory, in many cases, by using the criterion of the cavitation bubble length. A clear example is shown in Figure 47 by comparing the new design impeller B with the old design impeller A. It is evident that the bubble length ( $L_{c,b}$ ) was drastically reduced across the entire operating range. Moreover the suction recirculation point was also lowered down to 65 percent  $Q_{bep}$  (impeller B) from 90 percent (impeller A). Consequently, the cavitation erosion rate (ER) predicted with Equation (42) has been dramatically reduced as shown in Figure 48. New designs, impeller B and BM, are estimated to have a rate at least one order of magnitude less than the original old design, impeller A. Actual field data have proven that new design impeller B has largely exceeded the life target of 40,000 hours with life enhancement by a factor 3 to 6, as the old design impeller was heavily damaged within 14,000 hours (Unit 1) and 6000 hours (Unit 4). Moreover, the cavitation damage through the impeller hub with attack on the shaft caused by corner cavitation in the old impeller A was completely eliminated.

Similar successful and proven results of drastic enhancement for the impeller life with new hydraulic design approaches have been obtained by using different and effective features of the impeller geometry:

- Forward leaning blade leading edge (Bunjes, 1976),
- Optimized blade thickness distribution near leading edge (Hergt, 1991; Hergt, et al., 1996),

- Optimized vane shape from hub to tip plus forward leaning leading edge (Dijkers, et al., 2000).

All these new designs have indicated that the cavitation erosion associated with the mode of cavitation blade attached can be drastically reduced, while the cavitation damage caused by the corner cavitation has been in most cases eliminated.

An advanced impeller blade geometry has been developed by using a truly integrated design approach, which combines:

- Experimental flow visualization,
- Basic fluid dynamic considerations,
- Computational flow analysis, and
- Field experience with cavitation in high energy pumps.

This special impeller blade (patented) includes several new features (Cooper, et al., 1991; Sloteman, et al., 1991) includes:

- Elliptical nose on blades,
- Blade camber angle matched to analyzed flow,
- Biased-wedge blade thickness development,
- Biased-wedge blade thickness to avoid increase of  $NPSH_R$  due to loss of area between blades,
- Concave blade leading edge, blended forward.

The combination of the above features permits minimizing/eliminating the blade attached (sheet) cavitation in a wide range of duties plus eliminating the corner vortex cavitation. Also, pressure pulsations and noise level related with cavity volume are reduced, as proven by experimental data (Sloteman, et al., 2004).

The determination of the cavity length is a key step for predicting the cavitation erosion and making a sound assessment of the impeller life expectancy. As indicated above today, it is possible to predict the cavitation bubble length with CFD. However the CFD predictions need experimental verification to provide high confidence for the evaluation of the impeller life and associated probability. The validation of CFD results with experimental data is shown in Figures 10, 14, and 15 (Visser, 2001) with relation to  $NPSH_i$ , head curve versus  $NPSH_A$  and  $NPSH_3\%$ , respectively. An experimental validation directly associated with prediction of the cavitation bubble length under various cavitation levels has been published by Dupont (2001) covering five pumps with specific speed from 800 US to 6500 US. An example of the CFD validation is shown in Figure 54 for one pump ( $N_s = 1700$  US) and looks satisfactory.

It is worth noticing that CFD is presently used also for impeller design optimization in relation to cavitation performance, namely optimizing the  $NPSH_i$  curve (Torbergsen, et al., 2003; Elsasser and Brecht, 2006).

*Impeller Material*

It is known that the material resistance to cavitation has an important effect on the impeller life. In the correlation of cavitation erosion prediction given in Equation (42) the material resistance to cavitation erosion is related to the tensile strength  $R_m$ . However it is recognized that no unique material property (like hardness, tensile strength, etc.) is sufficient to describe the resistance to cavitation erosion (Gülich, 1989a) and presents a scatter over 100 percent when a wide range of alloys is considered. Actually literature information (Hammitt, 1980) indicates that ultimate resilience seems more appropriate than tensile strength or other material property to represent the resistance to cavitation but still with wide scatter.

It is also understood that the cavitation damage is a fatigue mechanism with specific characteristics that are not present with classical fatigue tests of material. Different test rigs have been used by individual companies to evaluate the material

resistance under cavitation attack. However the results appeared strictly dependent on the test rig and not transferable to actual pump cavitation conditions. ASTM G32 (1985) is the standard test method with material specimens for cavitation erosion using vibratory apparatus, which in the presence of liquid reproduces conditions of damaging cavitation (in the ultrasonic frequency range) comparable to damaging cavitation conditions inside an impeller. The test results of cavitation erosion rate given as MDP (MDP/T, T = time). These results are presented in Table 3 for various materials used in the pump industry along with the Brinell hardness number (BHN). Moreover the MDP values have been referred to the value for cast carbon steel ferritic and the inverse of the ratio  $MDP/MDP_{ref}$  is also shown in Table 3 with the name  $Imp\ Life/Imp\ Life_{ref}$ , which gives the relative life factor for a given material as compared to the reference material. Then Equation (42) can be used for all the materials listed in Table 3 by first making the life calculation with actual values for all input parameters and the reference material (i.e., using its corresponding  $R_m$  value), which is ferritic and requires material factor  $F_{mat} = 1$  as indicated by Gülich (1989a). Second, the impeller life for the specific material is obtained by multiplication with the ratio  $Imp\ Life/Imp\ Life_{ref}$ . In this way the material effect on impeller life is more directly representative of its resistance to cavitation attack as simulated with ASTM G32 (1985) than using the tensile strength value.

Table 3. Material Rating for Cavitation Erosion Resistance. (Courtesy of ASTM Standard G32, 1985)

Material	BHN	MDPR (Mils/Min)	Imp Life Imp Life <sub>ref</sub>
Stellite # 6 (Note 1)	444	0.00013	60.77
Stellite # 21 (Note 1)	292	0.00030	26.33
Stellite # 31 (Note 1)	265	0.00048	16.46
Stellite # 7 (Note 1)	292	0.00049	16.12
XM31-28.3 (X-Cav alloy)	260	0.00089	8.88
Wrought Nitronic 60 (Note 2)	212	0.00100	7.90
Waspoloy	N/A	0.00105	7.52
Inconel-718	388	0.00130	6.08
Maraging 300	N/A	0.00130	6.08
Manganese Steel	N/A	0.00190	4.16
Ti-6AL-4V	321	0.00220	3.59
Cast Nitronic 50	187	0.00240	3.29
CG3M mod. (Austenitic)	163	0.00290	2.72
Cast Ni-AL-BRZ	170	0.00340	2.32
Cast AL-BRZ	143	0.00360	2.19
Avesta 254SMO (Note 2)	170	0.00380	2.08
Ferralum 255 (Duplex)	255	0.00390	2.03
Cast CA15Cu (Note 3)	388	0.00400	1.98
17-4PH (cond. H1150)	255	0.00469	1.68
Wrought 316L (Note 2)	158	0.00570	1.39
Ductile NiResist	187	0.00640	1.23
Cast CF-3M (316L)	170	0.00650	1.22
Cast 15-5PH	277	0.00690	1.14
Cast CN7M	143	0.00720	1.10
Cast CA6NM	262	0.00740	1.07
<b>Cast Carbon Steel (Ferritic) *</b>	<b>166</b>	<b>0.00790</b>	<b>1.00</b>
Cast Inco 862 (HV93)	160	0.00880	0.90
Cast CA15 (410SS) (Martensitic)	217	0.01110	0.71
90-10 Copper Nickel	101	0.01950	0.41
Leaded Bronze	100	0.02130	0.37
Gray Cast Iron	200	0.04000	0.20

\* Reference Material  
 Note 1 - Primary use as wear resistant overlay. Not used as impeller casting alloy  
 Note 2 - Wrought material  
 Note 3 - CA15 modified with copper addition for higher hardness

In Table 3 the stellite alloys with various grades show the highest resistance to cavitation erosion. However these alloys can be applied as overlay with practical difficulties, but are not used for making impeller castings. A new alloy, which has presented cavitation resistance comparable to stellite (not

included in Table 3), is an austenitic stainless steel containing cobalt (trade name, Hydroloy®) and was used, successfully, as a weld filler metal to repair cavitation damage in hydraulic turbines (Simoneau, 1986). Field applications as a casting alloy were very limited because of casting and machinability problems for making impellers. However several impellers were installed in boiler feed pumps (McCaul, et al., 1993) replacing impellers made with CA6NM and providing much improved cavitation resistance.

A group of alloys that are used for producing impeller castings have been extracted from Table 3 and presented in Figure 56 by comparing the relative life factor Imp Life/Imp Life<sub>ref</sub>. It appears that alloy XM31-2&3 has the highest resistance to cavitation erosion with a relative impeller life factor close to 9. This is a chrome-manganese austenitic stainless steel casting alloy (McCaul, 1996) that combines superior cavitation resistance with the desired features of acceptable machinability and easy weldability allowing repair. All these characteristics make this material very suitable for successful industrial application as a pump impeller operating with cavitation. The first field application of this alloy, which was patented with the trade name X-Cavalloy™, was in 1994. Since that time the material has been used, mainly as an impeller, in many types of pump applications. Most have been as replacements for conventional materials that failed prematurely, due to cavitation damage. Some have been in new pump services, where NPSHA is only marginally higher than NPSHR, or other hydraulic design factors dictated the use of an impeller material with superior cavitation resistance to enhance the impeller life expectancy. Field experience with X-Cavalloy™ impellers (McCaul, 2004) confirms the laboratory cavitation test data (Table 3) suggesting that the impeller life can be extended, for many applications, by a factor of three or more (conservative assessment) in comparison with other conventional impeller materials.

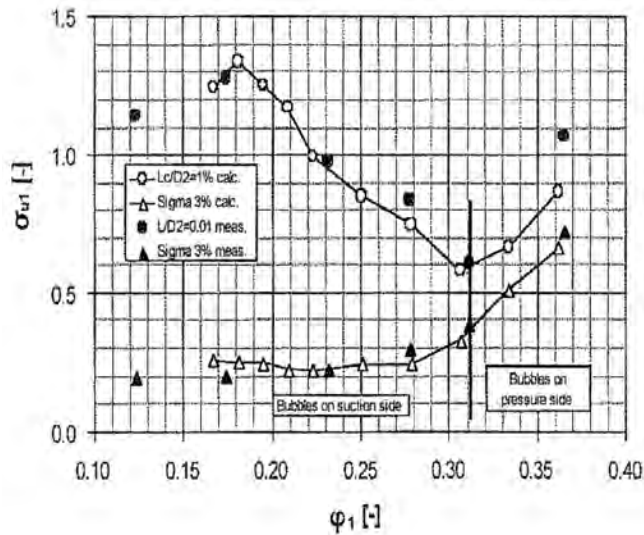


Figure 56. Predicted and Measured Cavity Lengths for a Radial Diffuser Pump of  $N_s = 2425$  US Units (Courtesy of Dupont, 2001, Turbomachinery Laboratory). Nondimensional NPSH Coefficient for Given  $L_c/D_2$  and 3 Percent Head Drop Versus Impeller Inlet Flow Coefficient.

Other commercially available materials can be chosen that can provide reasonable extension of the impeller life as shown in Figure 57, which can either give an urgent temporary remedy for field case solution or be combined with new impeller designs for achieving an enhanced impeller life with high probability of success.

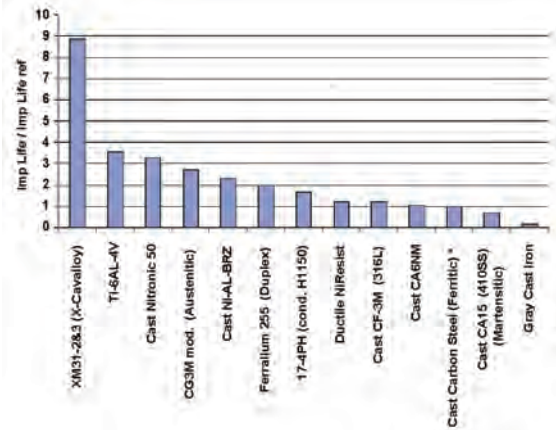


Figure 57. Impeller Life Ratio by Material Ranking for Cavitation Damage Resistance of Castable Alloys.

### CONCLUDING REMARKS

Cavitation is a phenomenon that can seriously impact performance and operation of pumps. Therefore it is important to have some understanding of the amount of cavitation that may occur in a particular situation; that is, for a given suction pressure (NPSH<sub>A</sub>). To that end, empirical correlations have been discussed that provide a means to predict:

- NPSH<sub>R</sub> for 40,000 hours impeller life time.
- Cavitation erosion.
- Influence of dissolved gases.
- Thermal depression.

It has further been outlined that computational fluid dynamics provides constructive means to get further insight in the performance to be expected under cavitation—enabling incipient NPSH characteristic, NPSH<sub>R</sub> (3 percent head drop), and cavitation bubble length to be determined from numerical simulation.

Enlightening literature data plus field information clearly point out that cavitation aspects affecting pump reliability are linked to pressure field. In particular, concerning the cavitation damage and the impeller life, the conventional NPSHR criterion based on 3 percent head drop, which is widely used in the industry, appears fully inadequate and even misleading at low flow operations below shockless capacity.

The most frequent cavitation modes that cause pump field problems, mostly characterized by metal damage and life reduction, have been discussed. The various basic flow mechanisms (sheet cavitation, suction recirculation vortex, corner vortex, impeller-diffuser/volute interaction, inlet flow distortion, inlet flow imbalance) have been interrelated with six and frequent cavitation modes, the pump geometry, and the operating conditions.

Highlights are presented about the key factors to be considered for establishing effective and economic NPSHA margins also underlining their relative ranking. Primary importance should be clearly assigned to the impeller eye peripheral velocity, impeller design, and operating capacity range, without ignoring other additional factors as listed. If these factors are correctly focused, then the role of the suction specific speed for NPSHA margins is marginal.

A key point is that with the present state-of-the-art, it is possible to control the cavitation intensity, namely the cavitation bubble length, within a wide operating range by new impeller design. Also, the erosion rate can be predicted for the normal operating range with some approximation by using either experimental data from cavitation visualizations and/or theoretical values from CFD simulations. Then it is possible to assess the impeller life expectancy, with a good probability of success. Furthermore, the

impeller life can be enhanced by using material with superior resistance to cavitation erosion.

## NOMENCLATURE

A	= 1 for cold water, 0.705 for boiler feedwater
B	= Vapor-to-liquid ratio
B <sub>1</sub>	= Thermodynamic effect parameter
C	= $7.92 \times 10^{-6} \text{ mm h}^{-1} \text{ Pa}^{-1}$ for blade suction side, $3.96 \times 10^{-4} \text{ mm h}^{-1} \text{ Pa}^{-1}$ for blade pressure side
C <sub>m1</sub>	= Meridional inlet velocity
E	= Erosion rate (mm/h)
f	= The scale factor
g	= Acceleration due to gravity
H	= Pump head
H <sub>V</sub>	= Vapor head
k <sub>1</sub>	= Constant = 1.2
k <sub>2</sub>	= $0.28 + (U_e \text{ [ft/s]}/400)^4$
L <sub>cav</sub>	= Bubble or cavity length
L <sub>cav,0</sub>	= Reference bubble length (10 mm)
n	= 2.83 for blade suction side, 2.6 for blade pressure side
N	= Rotational speed (rev/min)
NPSE	= Net positive suction energy = gNPSH
NPSH	= Net positive suction head
NPSH <sub>A</sub>	= Net positive suction head available
NPSH <sub>b</sub>	= Net positive suction head at head breakdown
NPSH <sub>i</sub>	= Incipient net positive suction head
NPSH <sub>R</sub>	= Net positive suction head required
NPSH <sub>SE,40</sub>	= Net positive suction head for 40,000 hour impeller life at shockless entry
NPSH <sub>40</sub>	= Net positive suction head for 40,000 hour impeller life
ΔNPSH	= NPSH <sub>R</sub> reduction due to dissolved gases
ΔNPSH <sub>40</sub>	= NPSH <sub>40</sub> increase due to incidence effect
NPSP	= Net positive suction pressure = $\rho g \text{NPSH}$
p <sub>1</sub>	= Upstream static pressure
p <sub>01</sub>	= Upstream total pressure
p <sub>E</sub>	= Effective or artificial vapor pressure
p <sub>V</sub>	= Vapor pressure
Q	= Volume flow rate
R	= Vapor-to-upstream-pressure ratio = $p_V / p_1$
R <sub>1T</sub>	= Impeller inlet vane-tip radius
S	= Suction specific speed = $\Omega Q^{1/2} / \text{NPSH}^{3/4}$
S <sub>0</sub>	= Reference or cold water value of suction specific speed
S <sub>b</sub>	= Suction specific speed at head breakdown
S <sub>i</sub>	= Suction specific speed at cavitation inception
s	= Solubility factor
t	= Blade thickness
t <sub>m</sub>	= (Mechanical) residence time or time available for cavitation development
T <sub>1</sub>	= Upstream temperature
T <sub>S</sub>	= Tensile strength
U <sub>e</sub>	= Peripheral velocity at impeller eye = $\Omega R_{1T}$
W <sub>1</sub>	= Relative inlet velocity
x <sub>G</sub>	= Mass fraction of dissolved gas
y	= Ratio of p <sub>E</sub> over p <sub>0</sub>
ρ	= Fluid density (kg/m <sup>3</sup> )
σ	= Cavitation number
σ <sub>d</sub>	= Desinent cavitation number
σ <sub>i</sub>	= Incipient cavitation number
σ <sub>TH</sub>	= Thoma cavitation number
σ <sub>TH,3%</sub>	= Thoma cavitation number at 3 percent head drop
τ <sub>A</sub>	= $2g\text{NPSH}_A / U_e^2$
Φ	= Specific flow rate = $Q / (\Omega R_{1T}^3)$
φ	= Inlet flow coefficient = $C_{m1} / U_e$
Ω	= Angular speed = $\pi N / 30$
Ω <sub>s</sub>	= Specific speed = $\Omega Q^{1/2} / (g H)^{3/4}$

## REFERENCES

- ANSI/HI 1.3, 2000, "American National Standard for Centrifugal Pumps for Design and Application," Hydraulic Institute, Parsippany, New Jersey, www.pumps.org.
- ANSI/HI 1.6, 2000, "American National Standard for Centrifugal Pump Tests," Hydraulic Institute, Parsippany, New Jersey, www.pumps.org.
- ANSI/HI 9.6.1, 1998, "American National Standard for Centrifugal and Vertical Pumps for NPSH Margin," Hydraulic Institute, Parsippany, New Jersey, www.pumps.org.
- ASTM Standard G32-85, 1985, "Standard Test Method for Cavitation Erosion Using Vibratory Apparatus," American Society for Testing and Materials, West Conshohocken, Pennsylvania.
- Arndt, R. E. A., 1981, "Cavitation in Fluid Machinery and Hydraulic Structures," *Annual Review of Fluid Mechanics*, 13, pp. 273-328.
- Boccazzi, A., Perdichizzi, A., Schiavello, B., and Tabacco, U., 1989, "Cavitation Behaviour and Internal Flow Measurements by Laser Doppler Anemometry in a Low Solidity Inducer," *Proceedings of the XXth Hydraulics Open Days on Hydraulic Machinery*, Lyon, France.
- Bunjes, J. H., 1976, "Design Principles and Test Data of Pump Impellers with Improved Cavitation Behaviour," *Improvements in Fluid Machines and Systems for Energy Conversion*, H. Worthington European Technical Award—1976, 4, Hoepli, Milan, Italy, pp. 185-212.
- Bunjes, J. H. and Op De Woerd, J., 1984, "Erosion Free Operation of Cavitating Pumps," *Proceedings of the 2nd European Congress on Fluid Machinery for the Oil, Petrochemical and Related Industries*, The Hague, The Netherlands, IMechE Conference Publications 1984-2, Paper C28, pp.1-12.
- Brennen, C. E., 1994, *Hydrodynamics of Pumps*, Oxford, England: Oxford University Press.
- Brennen, C. E., 1995, *Cavitation and Bubble Dynamics*, Oxford, England: Oxford University Press.
- Chen, C. C., 1982, "Cope with Dissolved Gases in Pump Calculations," *Chemical Engineering*, October, pp. 106-112.
- Chivers, T. C., 1967, "The Effect of Fluid Properties on Cavitation in a Centrifugal Pump," Thesis, University College, Cardiff, United Kingdom.
- Chivers, T. C., 1969, "Temperature Effects on Cavitation in a Centrifugal Pump: Theory and Experiment," *Proceedings of the Institution of Mechanical Engineers*, 184, Part 1, (2), pp. 37-47.
- Cooper, P. and Antunes, F. F., 1982, "Cavitation in Boiler Feed Pumps," *Proceedings of the Symposium on Power Plant Feed Pumps—The State of the Art*, EPRI CS-3158, Cherry Hill, New Jersey, pp. 24-29.
- Cooper, P., Sloteman, D. P., Graf, E., and Vlaming, D. J., 1991, "Elimination of Cavitation-Related Instabilities and Damage in High-Energy Pump Impellers," *Proceedings of the Eighth International Pump Users Symposium*, Turbomachinery Laboratory, Texas A&M University, College Station, Texas, pp. 1-20.
- Deeprise, W. M. and Herry, H., 1977, "The Effect of Size and Speed on Measured Pump Cavitation Performance," *Proceedings of the Conference on Scaling for Performance Prediction in Rotodynamic Machines*, University of Stirling, United Kingdom, IMechE Conference Publications 1977-7, Paper C187/77, pp. 123-130.

- Dernedde, R. and Stech, P. R., 1982, "Design of Feed Pumps Hydraulic Components," Proceedings of the Symposium on Power Plant Feed Pumps—The State of the Art, EPRI CS-3158, Cherry Hill, New Jersey, pp. 11-23.
- Dixon, S. L., 1978, *Fluid Mechanics, Thermodynamics of Turbomachinery*, Pergamon. Press.
- Dijkers, R. J. H., Visser, F. C., and Op de Woerd, J. G. H., 2000, "Redesign of a High-Energy Centrifugal Pump First-Stage Impeller," Proceedings of the Twentieth IAHR Symposium, Charlotte, North Carolina.
- Dupont, P., 2001, "Numerical Prediction of Cavitation in Pumps," *Proceedings of the Eighteenth International Pump Users Symposium, Turbomachinery Laboratory*, Texas A&M University, College Station, Texas, pp. 59-65.
- Elsasser, T. and Brecht, B., 2006, "The Gentle Giant of Niederaussem," *Pumps & Systems*, December, pp. 30-35.
- Ferman, R. S., Gopalakrishnan, S., Cugal, M., and Fuller, P. D. K., 1997, "Boiler Feed Pump Re-rate for Increased Head and Reduced Cavitation," Proceedings of the ASME Third International Symposium on Pumping Machinery, Vancouver, Canada.
- Florjancic, D., 1982, "Developments and Design Requirements for Modern Boiler Feed Pumps," Proceedings of the Symposium on Power Plant Feed Pumps—The State of the Art, EPRI CS-3158, Cherry Hill, New Jersey, pp. 74-99.
- Franc, J. P. and Michel, J. M., 2004, *Fundamentals of Cavitation*, Kluwer Academic Publishers.
- Gongwer, A. C., 1941, "A Theory of Cavitation Flow in Centrifugal-Pump Impellers," *Transactions of ASME*, 63, pp. 29-40.
- Grist, E., 1974, "Net Positive Suction Head Requirements for Avoidance of Unacceptable Cavitation Erosion in Centrifugal Pumps," Cavitation, Fluid Machinery Group, Heriot-Watt University, Edinburgh, Scotland, IMechE Conference Publication CP13-1974, London, England, Paper C163-74.
- Gulich, J. F., 1987, "Influence of Interaction of Different Components on Hydraulic Pump Performance and Cavitation," Proceedings of the Symposium on Power Plant Feed Pumps, EPRI CS-5857, New Orleans, Louisiana, pp. 2-75 to 2-96.
- Gulich, J. F., 1989a, "Guidelines for Prevention of Cavitation in Centrifugal Feedpumps," EPRI Final Report GS-6398.
- Gulich, J. F., 1989b, "Beitrag zur Bestimmung der Kavitationserosion in Kreiselpumpen auf Grund der Blasenfeldlänge und des Kavitationsschalls," Dissertation Technische Hochschule Darmstadt, Germany.
- Gulich, J. F., 1992, "Diagnosis of Cavitation in Centrifugal Pumps," *World Pumps*, May, pp. 13-20.
- Gulich, J. F., 2001, "Selection Criteria for Suction Impellers of Centrifugal Pumps," *World Pumps*, January, pp. 28-34.
- Gulich, J. F. and Pace, S., 1986, "Quantitative Prediction of Cavitation Erosion in Centrifugal Pumps," Proceedings of the Thirteenth IAHR Symposium on Progress in Technology, Montreal, Canada, Paper 42.
- Gulich, J. F. and Rösch, A., 1988, "Cavitation Erosion in Centrifugal Pumps," *World Pumps*, July, pp. 164-168.
- Hallam, J. L., 1982, "Centrifugal Pumps: Which Suction Specific Speeds Are Acceptable?," *Hydrocarbon Processing*, April.
- Hammitt, G. F., 1963, "Observation of Cavitation Scale and Thermodynamic Effects in Stationary and Rotating Components," *Transactions of ASME Journal of Basic Engineering*, 85, pp. 1-16.
- Hammitt, G. F., 1980, *Cavitation and Multiphase Flow Phenomena*, McGraw-Hill Inc.
- Hammitt, G. F. and Rogers, D. O., 1970, "Effects of Pressure and Temperature Variation in Vibratory Cavitation Damage Test," *Journal Mechanical Engineering Science*, 12, (6), pp. 432-439.
- Hergt, P., 1991, "Design Approach for Feed Pump Suction Impellers," Proceedings of EPRI Symposium on Power Plant Pumps, Tampa, Florida.
- Hergt, P., Nicklas, A., Moellenkopf, G., and Brodersen, S., 1996, "The Suction Performance of Centrifugal Pumps Possibilities and Limits of Improvements," *Proceedings of the Thirteenth International Pump Users Symposium*, Turbomachinery Laboratory, Texas A&M University, College Station, Texas, pp. 13-25.
- Kercan, V. and Schweiger, F., 1979, "Cavitation Phenomena Detection by Different Methods," Proceedings of the 6th Conference on Fluid Machinery, Akademiai Kiado, Budapest, Hungary, pp. 535-543.
- McCaul, C., 1996, "An Advanced Cavitation Resistant Austenitic Stainless Steel for Pumps," *Corrosion 96*, Denver, Colorado, NACE International, Paper 415.
- McCaul, C., 2004, "A Cavitation-Resistant Casting Alloy for Pumps—Status after Ten Years' Commercial Use," Proceedings of the Institution of Mechanical Engineers, Second International Symposium on Advanced Materials for Fluid Machinery, London, United Kingdom, IMechE Conference Transactions 2004-1, Paper S965/002/2004.
- McCaul, C., Schiavello, B., and Dawson, R., 1993, "A New Highly Cavitation Resistant Casting Alloy and Its Application in Pumps," *NACE—Corrosion '93*, New Orleans, Louisiana.
- McNulty, P. J. and Pearsall, I. S. 1979, "Cavitation Inception in Pumps" Proceedings of the ASME International Symposium on Cavitation Inception, New York, New York, pp. 163-170.
- McNulty, P. J. and Pearsall, I. S., 1982, "Cavitation Inception in Pumps," *Transactions of ASME Journal of Fluids Engineering*, 104, pp. 99-104.
- Minami, S., Kawaguchi, K., and Homma, T., 1960, "Experimental Investigation on Cavitation in Centrifugal Pump Impellers," *Bulletin of JSME*, 3, (9), pp. 9-19.
- Okamura, T. and Miyashiro, H., 1978, "Cavitation in Centrifugal Pumps Operating at Low Capacities," *Polyphase Flow in Turbomachinery*, ASME Winter Annual Meeting, San Francisco, California, pp. 243-251.
- Okamura, T., Ohki, H., and Matsunaga, Y., 1985, "Intensity of Cavitation Erosion in Centrifugal Pumps Operating at Low Capacities," Proceedings of Cavitation in Hydraulic Structures and Turbomachinery, The Joint ASCE/ASME Mechanics Conference, Albuquerque, New Mexico, ASME FED 25, pp. 63-70.
- Schiavello, B., 1982, "Critical Flow Engendering Appearance of Recirculation at Centrifugal Pump Impeller Inlet: Determinant Phenomena, Detection Methods, Forecasting Criteria," *La Houille Blanche*, 2/3, pp. 139-158 (in French).
- Schiavello, B., 1986, "Visual Study of Cavitation—An Engineering Tool to Improve Pump Reliability," Proceedings of EPRI 1st International Conference on Improved Coal-Fired Power Plants, Palo Alto, California.
- Schiavello, B., 1992, "Cavitation and Recirculation Field Problems" Presented but not published, The Ninth International Pump Users Symposium, Turbomachinery Laboratory, Texas A&M University, College Station, Texas.

- Schiavello, B., 1993, "Cavitation and Recirculation Troubleshooting Methodology," *Proceedings of the Tenth International Pump Users Symposium*, Turbomachinery Laboratory, Texas A&M University, College Station, Texas, pp. 133-156.
- Schiavello, B. and Prescott, M., 1991, "Field Cases Due to Various Cavitation Damage Mechanisms: Analysis and Solutions," *Proceedings of EPRI Symposium on Power Plant Pumps*, Tampa, Florida.
- Schiavello, B. and Sen, M., 1980, "On the Prediction of the Reverse Flow Onset at the Centrifugal Pump Inlet," *Proceedings of Performance Prediction of Centrifugal Pumps and Compressors*, ASME 22nd Annual Fluids Engineering Conference, New Orleans, Louisiana, pp. 261-272.
- Schiavello, B. and Sen, M., 1981, "Experimental Investigation on Centrifugal Pump Design Criteria for Minimum Reverse Flow Delivery," *Improvements in Turbomachines and Related Techniques*, H. Worthington European Technical Award—1979, 5, Hoepli, Milan, Italy, pp. 191-239.
- Schiavello, B., Arisawa, T., and Marengo, G., 1988, "Flow Visualization—A Design Tool to Improve Pump Cavitation Performance," *Proceedings of the 2nd International Symposium on Transport Phenomena, Dynamics and Design of Rotating Machinery*, Honolulu, Hawaii, pp. 484-449.
- Schiavello, B., Marengo, G., and Arisawa, T., 1988, "Improvement of Cavitation Performance and Impeller Life in High Energy Boiler Feed Pump," *Proceedings of the 14th IAHR Symposium on Progress Within Large and High Specific Energy Units*, Trondheim, Norway, Paper J3.
- Scott, C. and Ward, T., 1992, "Cavitation in Centrifugal Pump Diffusers," *Proceedings of the Institution of Mechanical Engineers—International Conference on Cavitation*, Robinson College, Cambridge, United Kingdom, IMechE Conference Publications 1992-11, Paper C453/033, pp. 103-110.
- Simoneau, R., 1986, "A New Class of High Strain Hardening Austenitic Stainless Steel to Fight Cavitation Erosion," *Proceedings of the Thirteenth IAHR Symposium on Progress in Technology*, Montreal, Canada, Paper 83.
- Sloteman, D. P., Cooper, P., and Graf, E., 1991, "Design of High-Energy Pump Impellers to Avoid Cavitation Instabilities and Damage," *Proceedings of EPRI Symposium on Power Plant Pumps*, Tampa, Florida.
- Sloteman, D. P., Robertson, D. A., and Margolin, L., 2004, "Demonstration of Cavitation Life Extension for Suction-Stage Impellers in High Energy Pumps," *Proceedings of the Twenty-First International Pump Users Symposium*, Turbomachinery Laboratory, Texas A&M University, College Station, Texas, pp. 103-115.
- Steller, K., 1983, "Prediction of Cavitation Damage in Hydraulic Turbomachinery," *Proceedings of the 7th Conference on Fluid Machinery*, Akademiai Kiado, Budapest, Hungary, pp. 846-855.
- Stepanoff, A. J., 1965, *Pumps and Blowers—Two-Phase Flow*, John Wiley & Sons.
- Tomita, Y., Shima, A., and Takahashi, K., 1983, "The Collapse of Gas Bubble Attached to a Solid Wall by a Shock Wave and Induced Impact Pressure," *Transactions of ASME Journal of Fluids Engineering*, 105, pp. 341-349.
- Torbergsen, E., Gjerstadt, S., Hosøy, A., and Aasland, B., 2003, "Cavitation Study in a High Pressure Water Injection Pump," *Proceedings of the Twentieth International Pump Users Symposium*, Turbomachinery Laboratory, Texas A&M University, College Station, Texas, pp. 49-55.
- Tsai, M. J., 1982, "Accounting for Dissolved Gases in Pump Design," *Chemical Engineering*, July, pp. 65-69.
- Van Der Westhuizen, 1992, "Cavitation Erosion Effects Due to Off Design Operation of Boiler Feed Pumps in 600 MW Power Stations," *Proceedings of the Institution of Mechanical Engineers—International Conference on Cavitation*, Robinson College, Cambridge, United Kingdom, IMechE Conference Publications 1992-11, Paper C453/022, pp. 249-262.
- Vlaming, D. J., 1981, "A Method for Estimating the Net Positive Suction Head Required by Centrifugal Pumps," ASME Paper No. 81-WA/FE-32.
- Vlaming, D. J., 1989, "Optimum Impeller Inlet Geometry for Centrifugal Pumps," *Proceedings of the ASME First International Symposium on Pumping Machinery*, San Diego, California, pp. 25-29.
- Visser, F. C., 2001, "Some User Experience Demonstrating the Use of Computational Fluid Dynamics for Cavitation Analysis and Head Prediction of Centrifugal Pumps," *Proceedings of the Fourth ASME International Symposium on Pumping Machinery*, New Orleans, Louisiana. Paper No. FEDSM2001-18087.
- Visser, F. C., Backx, J. J. M., Geerts, J., Cugal, M., and D. Miguel Median Torres, 1998, "Pump Impeller Lifetime Improvement Through Visual Study of Leading-Edge Cavitation," *Proceedings of the Fifteenth International Pump Users Symposium*, Turbomachinery Laboratory, Texas A&M University, College Station, Texas, pp. 109-117.
- Wislicenus, G. F., Watson, R. M., and Karassik I. J., 1939, "Cavitation Characteristics of Centrifugal Pumps Described by Similarity Considerations," *Transactions of ASME*, 61, pp. 17-24. (Paper Discussion: 1940 - *Transactions of ASME*, 62, pp. 155-166.)
- Wood, D. W., Hart, R. J., and Marra, E., 1998, "Application Guidelines for Pumping Liquids That Have a Large Dissolved Gas Content," *Proceedings of the Fifteenth International Pump Users Symposium*, Turbomachinery Laboratory, Texas A&M University, College Station, Texas, pp. 91-98.
- Wood, G. M., 1963, "Visual Cavitation Studies of Mixed Flow Pump Impellers," *Transactions of ASME Journal of Basic Engineering*, 85, pp. 17-28.
- Wood, G. M., Murphy, J. S., and Farquar, J., 1960, "An Experimental Study of Cavitation in a Mixed Flow Pump Impeller," *Transactions of ASME Journal of Basic Engineering*, 82, pp. 929-940.
- Worster, R. C., 1963, "The Flow in Volute and its Effect on Centrifugal Pump Performance," *Proceedings of the Institution of Mechanical Engineers*, 177, (31), pp. 843-875.

#### ACKNOWLEDGEMENT

The authors wish to thank the management of Flowserve for their support and permission to publish this material and present the tutorial.